JCB Journal of Cell Biology

ARTICLE

eIF5A controls mitoprotein import by relieving ribosome stalling at *TIM50* translocase mRNA

Marina Barba-Aliaga[1,2,3], Vanessa Bernal[1,2], Cynthia Rong[3], Madeleine E. Volfbeyn[3], Keguang Zhang[3], Brian M. Zid[3], and Paula Alepuz[1,2]

Efficient import of nuclear-encoded proteins into mitochondria is crucial for proper mitochondrial function. The conserved translation factor eIF5A binds ribosomes, alleviating stalling at polyproline-encoding sequences. eIF5A impacts mitochondrial function across species, though the precise molecular mechanism is unclear. We found that eIF5A depletion in yeast reduces the translation and levels of the TCA cycle and oxidative phosphorylation proteins. Loss of eIF5A causes mitoprotein precursors to accumulate in the cytosol and triggers a mitochondrial import stress response. We identify an essential polyproline protein as a direct target of eIF5A: the mitochondrial inner membrane protein and translocase component Tim50. Thus, eIF5A controls mitochondrial protein import by alleviating ribosome stalling along Tim50 mRNA at the mitochondrial surface. Removal of polyprolines from Tim50 partially rescues the mitochondrial import stress response and translation of oxidative phosphorylation genes. Overall, our findings elucidate how eIF5A impacts the mitochondrial function by promoting efficient translation and reducing ribosome stalling of co-translationally imported proteins, thereby positively impacting the mitochondrial import process.

Introduction

Mitochondria are complex eukaryotic organelles with endosymbiotic origin (Roger et al., 2017). In eukaryotes, mitochondria are essential for energy production and macromolecular synthesis as they house key metabolic processes such as oxidative phosphorylation (OXPHOS), electron transport chain (ETC), or tricarboxylic acid (TCA) cycle, and lipid, amino acids, heme, and Fe-S clusters synthesis. Besides, mitochondria also participate in other cellular processes including Ca^{+2} homeostasis and apoptosis. Given its cellular essentiality, mitochondrial function is critical in health and disease and is a pivotal hallmark of aging-related disorders (Balaban et al., 2005; Boengler et al., 2017).

The mitochondrial proteome comprises about 1,000 proteins in budding yeast (Schmidt et al., 2010). While the mitochondrial genome encodes 1% of them, the other 99% are encoded in the nuclear genome (Borst and Grivell, 1973). Therefore, these nuclear-encoded mitochondrial proteins, herein termed mitoproteins, need to be transported into the mitochondria to fulfill their biological function. Mitoprotein import is therefore a key process for optimal mitochondrial function (Bykov et al., 2020). Mitoproteins are imported into the mitochondria through both post- and co-translational mechanisms. In the first case, cytosolic chaperones bind to and keep mitoproteins in an unfolded import-competent conformation until delivered to receptors at the mitochondrial surface (Hansen and Herrmann, 2019). Co-translational translocation implies the coupling of synthesis and import, with mRNA localization to the mitochondrial surface (Kellems and Butow, 1972; Williams et al., 2014; Tsuboi et al., 2020).

Protein translocases in the mitochondrial outer and inner membrane (MOM and MIM) mediate the import and sorting of proteins into mitochondria. Mitoproteins initially enter the organelle through the general translocase of the outer membrane (TOM complex), known as the universal entry gate. Most mitoproteins are recognized by their N-terminal positively charged presequences, the most common mitochondrial targeting sequences (MTS) (Vögtle et al., 2009). Usually, mitoproteins contact the central receptor Tom20 and cross to the intermembrane space (IMS) through Tom40, the β-barrel pore-forming subunit. Mitoproteins targeting the MIM or the mitochondrial matrix (MM) are then recognized by the major translocase of the inner membrane (TIM23 complex), with Tim23 as the central subunit and translocase pore and Tim50 as the receptor protein that specifically recognizes the MTS. TIM translocation is energetically driven by the MIM membrane potential and the action of the mtHsp70 motor system. Once reaching their destination, the MTS sequence is cleaved and the

[1]Instituto de Biotecnología y Biomedicina (Biotecmed), Universitat de València, València, Spain; [2]Departamento de Bioquímica y Biología Molecular, Facultad de Ciencias Biológicas, Universitat de València, València, Spain; [3]Department of Chemistry and Biochemistry, University of California San Diego, La Jolla, CA, USA.

Correspondence to Paula Alepuz: paula.alepuz@uv.es; Marina Barba-Aliaga: marina.barba@uv.es; Brian M. Zid: zid@ucsd.edu.

protein is folded. Mitoproteins with no MTS show unclear targeting signals and their import is mediated by other translocases (see reviews Wiedemann and Pfanner, 2017; Lenkiewicz et al., 2022; Haastrup et al., 2023).

Import failure of mitoproteins leads to proteotoxic effects inside and outside the mitochondria, as unfolded precursors accumulate on the translocases and in the cytosol, which is detrimental to cellular fitness and is associated with various diseases. However, yeast cells are equipped with several stress responses which include transcriptional and translational reprogramming, reducing the protein synthesis, and increasing proteasomal activity to remove accumulated precursors from translocases and cytosol (Wang and Chen, 2015; Wrobel et al., 2015; Boos et al., 2019; Weidberg and Amon, 2018; Mårtensson et al., 2019).

Eukaryotic translation initiation factor 5A (eIF5A) is an essential and highly conserved protein across eukaryotes and *archaea* (Schnier et al., 1991). eIF5A promotes the translation elongation not only between amino acids known to be poor substrates for the formation of peptide bonds that may stall translation, such as polyproline motifs, but also combinations of proline, glycine, and charged amino acids (Gutierrez et al., 2013; Pelechano and Alepuz, 2017; Schuller et al., 2017). eIF5A is the only known cellular protein containing the posttranslational and essential modification hypusine, and in most eukaryotes, it is codified by two highly homologous isoforms, *TIF51A* and *TIF51B* in yeast (Jenkins et al., 2001; Park et al., 2021). eIF5A expression is regulated according to the metabolic demands of the cell. In yeast, *TIF51A* gene is upregulated under respiratory conditions by the transcription (activator/repressor) factor Hap1 (Barba-Aliaga et al., 2020; Barba-Aliaga and Alepuz, 2022a), which responds to changes in oxygen and heme levels to activate the transcription of many respiratory genes (Zhang and Hach, 1999). However, under hypoxic/non-respiratory conditions, Hap1 represses *TIF51A* expression (Barba-Aliaga et al., 2020; Barba-Aliaga and Alepuz, 2022a).

The cellular adaptation of eIF5A expression according to the energetic status of the cell highlights the essential role of eIF5A in mitochondrial function. Thus, a reduction in eIF5A protein triggers a decrease in the mitochondrial respiration rate and its membrane potential (Barba-Aliaga et al., 2020; Barba-Aliaga and Alepuz, 2022a, 2022b; Melis et al., 2017; Giraud et al., 2020). In addition, mitochondrial localization of eIF5A has been reported (Liu et al., 2012; Miyake et al., 2015; Pereira et al., 2016). Until now, two alternative but related mechanisms to explain the eIF5A role in mitochondrial function have been described. First, eIF5A was reported to control the synthesis and activity of many mitoproteins of macrophage cells. The MTSs of some of them were sufficient to confer hypusinated eIF5A-dependent translation efficiency, suggesting that eIF5A might regulate mitochondrial activity by promoting, directly or indirectly, the translation of MTSs of some mitoproteins, which are rich in charged amino acids (Puleston et al., 2019). In connection with this, Zhang et al. (2022) reported how eIF5A promotes the translation of some yeast respiratory proteins in response to oxygen levels and suggested that eIF5A and its hypusine would favor a suitable interaction between the amino acids from the MTSs regions and the peptide exit tunnel. Here, we describe an alternative molecular mechanism by which eIF5A promotes mitochondrial activity. Our findings demonstrate that eIF5A plays a crucial role in maintaining mitochondrial function by alleviating ribosome stalling during the translation of the co-translationally imported protein Tim50. This mechanism is essential for efficient mitochondrial protein import and translocation. We observed that depletion of eIF5A triggers a cascade of events: accumulation of precursor proteins in the cytosol, activation of the mitochondrial import stress response, and a subsequent reduction in the translation and levels of many mitochondrial proteins. By specifically facilitating the translation of Tim50 and other similar proteins, eIF5A prevents the initiation of this stress response, thereby ensuring proper mitochondrial protein import and maintaining overall mitochondrial health and function. This newly discovered role of eIF5A represents a distinct pathway through which it contributes to cellular homeostasis, particularly in the context of mitochondrial activity.

Results

Depletion of eIF5A results in the downregulation of many mitochondrial proteins including components of OXPHOS, TCA, and mitochondrial membrane transporters

We and others have found that eIF5A is necessary to maintain high mitochondrial activity; additionally, several mitoproteins whose levels drop in the absence of functional eIF5A have been identified in yeast and mammalian cells (Puleston et al., 2019; Barba-Aliaga et al., 2020; Barba-Aliaga and Alepuz, 2022a; Zhang et al., 2022). To expand our knowledge on the role of eIF5A in mitochondria, we performed a proteomic experiment in which wild-type and two eIF5A temperature-sensitive mutant yeast strains, *tif51A-1* carrying a single point mutation (Pro83 to Ser), and *tif51A-3* carrying a double point mutation (Cys39 to Tyr, Gly118 to Asp) (Li et al., 2011, 2014) were exponentially grown in YPD media at 25°C and then incubated at 41°C for 4 h to get a strong depletion of eIF5A. Data from the three replicates shown in the multidimensional scaling (MDS)-plot indicated that eIF5A mutants are already different in their proteome with respect to the wild-type at permissive temperature, and this difference is exacerbated at restrictive temperature (Fig. S1 A). We also confirmed the response of wild-type to heat stress conferred by incubation at 41°C as there was an enrichment in the functional categories (Gene Ontology [GO]) of "Cellular response to stress" in its upregulated proteins (Fig. S1 C). We calculated the 41°C/25°C fold change of protein levels and then the ratios between this fold change for each mutant with respect to the wild-type. Out of the 1,358 proteins detected in the three strains, 292 were significantly downregulated and 135 upregulated in at least one mutant with respect to the wild-type (138 down- and 38 upregulated in both eIF5A mutants). Downregulated proteins were enriched in several functional categories related to mitochondria (Fig. S1 D and Table S1), including OXPHOS proteins and TCA enzymes (Fig. 1, A and B; and Table S1). We observed that several mitochondrial membrane transporters were also downregulated, as the phosphate (Mir1) and the ADP/ATP (Pet9)

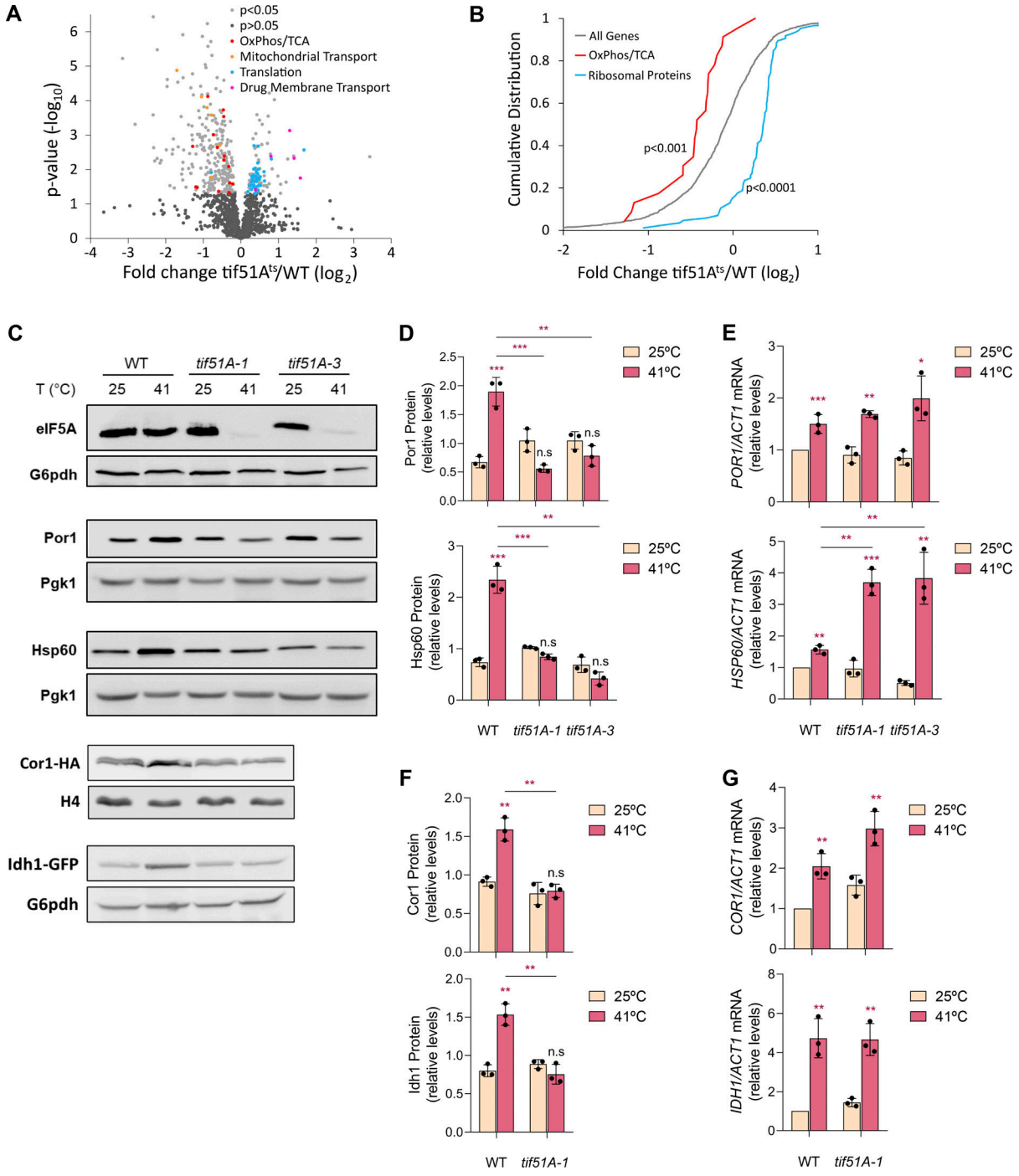

Figure 1. **Proteomic analysis of eIF5A depletion shows downregulation of mitochondrial proteins. (A)** Volcano plot showing the log_2 fold change values (*tif51A^{ts}* relative to wild-type) of 1,358 detected proteins plotted against their associated $-log_{10}$ P values. *tif51A^{ts}* stands for the average values obtained for the two eIF5A temperature-sensitive strains (*tif51A-1* and *tif51A-3*). Dots representing individual proteins were divided in five different groups: P value >0.05 (black); P value <0.05 (grey); OXPHOS/TCA proteins (red); mitochondrial transport proteins (orange); translation proteins (blue); and drug membrane transport proteins (magenta). **(B)** Cumulative distributions of log_2 fold changes of all proteins detected (grey), OXPHOS/TCA (red), and ribosomal proteins (blue). **(C–G)** Wild-type, *tif51A-1*, and *tif51A-3* strains were cultured in YPD at 25°C until the early exponential phase and transferred to 25°C or 41°C for 4 h. eIF5A, Por1, Hsp60, Cor1, and Idh1 protein levels were determined by western blotting (C) and quantified (D and F). G6pdh levels were used as loading control. A representative image is shown from three independent experiments. **(E and F)** *POR1*, *HSP60*, *COR1*, and *IDH1* mRNA relative levels were determined by RT-qPCR. Data information: In D–G, results are presented as mean ± SD from three independent experiments. The statistical significance was measured by using a two-tailed paired Student's *t* test. *P < 0.05, **P < 0.01, ***P < 0.001. The asterisks located above the columns of the graph represent a comparison between 41°C and 25°C conditions within the same strain. The asterisks found at the top of the bars additionally indicate comparisons between the indicated strains at the same treatment condition. n.s means no significant differences. Source data are available for this figure: SourceData F1.

MIM carrier proteins and receptor members of the TOM translocase of the MOM (Tom20, Tom70) (Fig. 1, A and B; and Fig. S1 D and Table S1). To independently corroborate the proteomic results, we confirmed the reduction in the levels of several downregulated mitoproteins, the Por1 porin of the MOM, the Hsp60 chaperone of the MM, the Cor1 component of the MIM ETC, and the Idh1 NAD^+-dependent isocitrate dehydrogenase of the TCA cycle in both *tif51A-1* and *tif51A-3* mutants at the restrictive temperature (Fig. 1, C, D, and F), with no changes in mRNA levels (Fig. 1, E and G). On the other hand, proteins of functional categories related to cytoplasmic translation were upregulated in eIF5A mutants with respect to wild-type due to a lower decrease in the 41°C/25°C fold change in the eIF5A mutants (Fig. 1, A and B; and Fig. S1 D). Proteins of the category "drug membrane transport" (Snq2, Yor1, Qdr2, Pdr5) were also upregulated in the eIF5A mutants at 41°C (Fig. 1 A, Fig. S1 D, and Table S1). In sum, the proteomic results indicated, among other effects, the requirement of eIF5A to maintain adequate protein levels of a wide range of mitoproteins.

Although depleting eIF5A via temperature-sensitive mutants is usually performed at 37°C (Li et al., 2014; Pelechano and Alepuz, 2017), we have used herein a highly restrictive temperature (41°C) to achieve a robust depletion of eIF5A. Nonetheless, we validated a similar growth impairment and eIF5A protein depletion in the two temperature-sensitive mutants at both temperatures, along with a significant reduction of the mitoprotein Por1 compared with wild-type at both 37°C and 41°C (Fig. S1, B and E).

An important outcome of our proteomic analysis was that among the downregulated mitoproteins upon eIF5A depletion, most of them did not contain consecutive prolines nor a high number of other eIF5A-dependent motifs in their sequences (Pelechano and Alepuz, 2017; Schuller et al., 2017) (Table S1). This finding had been previously observed in yeast and mammalian cells (Puleston et al., 2019; Zhang et al., 2022) and suggests a general downregulation of mitochondrial protein levels in the absence of eIF5A and, thus, a role for eIF5A different from that well-described and direct one on translating problematic amino acids for peptide bond formation.

eIF5A depletion causes a downregulation of mitochondrial protein translation

The specific decrease in the levels of mitoproteins upon eIF5A depletion could be explained by decreased translation of the corresponding mRNAs, as it is suggested by similar or even higher mRNA levels of the downregulated proteins Por1, Hsp60, Cor1, and Idh1 in *tif51A-1* and *tif51A-3* mutants (Fig. 1, E and G). To further investigate if the general downregulation of mitoproteins occurred at the translational level, we obtained polysome profiles for wild-type and *tif51A-1* strains in galactose media to promote respiration at both permissive (25°C) and restrictive (37°C) temperatures and determined the distribution of specific mRNAs among the different polysomal fractions. Importantly, polysomes were maintained in both strains at both temperatures, indicating that global translation was not significantly affected (Fig. 2, A and B). Based on the specific mRNA profiles obtained by quantitative PCR (qPCR) analysis, we decided to classify the mRNAs for analysis as short (<600 bp) or long (>600 bp) ORF length mRNAs (Table S5 and detailed explanation in Materials and Methods section). To analyze the distribution of short length RNAs along the fractions, we divided the polysome profiles into three different sections corresponding to the monosomal fractions (M), light fractions occupied by mRNAs with 2 or 3 ribosomes (2n-3n), and the rest of the heavy polysomal fractions (P). For long-length RNAs, we used the sections corresponding to the monosomal fractions (M), fractions with 2–8 ribosomes (2n-8n) and the rest of the heavy polysomal fractions (P) (Fig. S2 A). In agreement with unaffected global translation, we found no differences in the ratios P/2n-3n and P/2n-8n between the two strains at both permissive and restrictive temperatures (Fig. S2, B and C).

Next, we investigated the distribution of mRNAs encoding for mitoproteins with different biological functions and intramitochondrial localization (Table S5). Since no differences were found in the monosomal fractions upon eIF5A depletion (Fig. S2, D–I), we calculated the fold change between the mRNA abundance found at heavy and light polysomal fractions. Significant lower ratios were observed for *PET9*, *TOM20*, and *TOM70* mRNAs encoding mitochondrial transporters (ADP/ATP carrier and receptors of the TOM complex, respectively) at the MIM and MOM in the *tif51A-1* strain at restrictive temperature (Fig. 2 C and Fig. S2 D), with no significant differences at permissive temperature (Fig. S2 G). These results indicated that the mRNA abundance was shifted to earlier fractions and translation was reduced. Similar results were observed for the *ATP1*, *CYC1*, and *COX5A* mRNAs encoding OXPHOS components at the MM, IMS and MIM, respectively (Fig. 2 C; and Fig. S2, E and H). The statistically significant movement toward the lighter fractions is indicative of translation downregulation but it could be alternatively indicative of the stall of ribosomes in the 5′ ORF regions and/or at the predicted MTS (Table S5). The reported lower ribosome association with the mitochondrial mRNAs upon eIF5A depletion was in agreement with our proteomic analyses since seven out of the eight tested mRNAs encoding for mitoproteins were detected in the proteomic study and showed downregulation of the protein levels in the two eIF5A mutants at the restrictive temperature (Table S1).

We also studied the translation of the constitutively expressed *ACT1*, *RPP2B*, and *EFT2* mRNAs encoding actin, a ribosomal protein and translation elongation factor, respectively, localized in the cytosol. Similar ratios were found between the wild-type and *tif51A-1* strains at both temperatures, indicating that the translation of these mRNAs remained unaffected in the absence of eIF5A (Fig. 2 C; and Fig. S2, F and I), which agrees with the finding that global translation is not affected in the *tif51A-1* mutant (Fig. S2, B and C).

To specifically address whether the synthesis of mitoproteins by translation is downregulated upon eIF5A depletion, we used a reporter construct integrated into the *URA3* locus, consisting of a $tetO_7$ inducible promoter and a nanoluciferase (nLuc) reporter ORF for measuring the kinetics of protein synthesis. This system was recently used to quantify protein levels and translation stall duration from reporter mRNAs in yeast (Hou et al., 2023). We

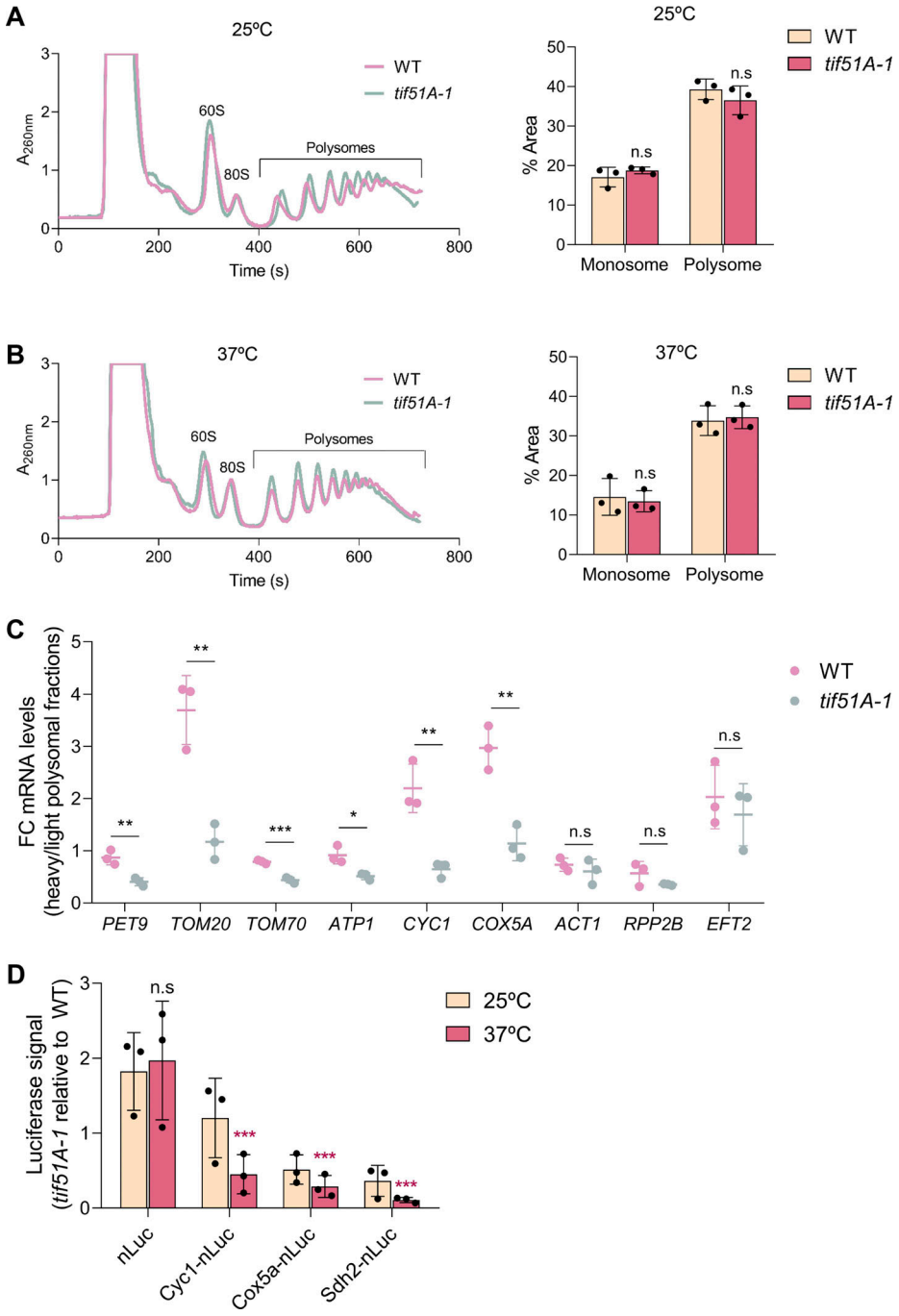

Figure 2. **The levels of mitochondrial proteins are post-transcriptionally affected upon eIF5A depletion. (A and B)** Polysome profiles were obtained for wild-type and *tif51A-1* strains cultured in SGal at 25°C (A) or 37°C (B) for 4 h. A representative profile is shown from three independent experiments (left). The average polysome and monosome area is represented for each strain at both temperatures (right). **(C)** The RNA from individual fractions of the polysome profiles was extracted and the mRNA levels were analyzed by RT-qPCR using gene-specific primers in the corresponding sections at restrictive temperature. Fold change (FC) between the heavy and the low polysomal sections are presented. **(D)** Wild-type strain and *tif51A-1* expressing nLuc, Cyc1-nLuc, Cox5a-nLuc, or Sdh2-nLuc (from left to right) reporters were cultured in YPD until early exponential phase and then transferred to 25°C or 37°C for 4 h. After addition of doxycycline to induce luciferase expression, the luminescence levels generated by the nLuc 60 min after the addition of the furimazine substrate were measured. Data information: In A–D, results are presented as average ± SD from three independent experiments. The statistical significance was measured by using a two-tailed paired Student's *t* test. *P < 0.05, **P < 0.001, ***P < 0.001. n.s means no significant differences.

generated fusions of the OXPHOS genes *CYC1* and *COX5A* and the TCA enzyme *SDH2* to the nLuc reporter gene. After inducing expression, we analyzed the protein synthesis by incubating for 1 h in anhydrotetracycline-supplemented media. We did not find significant differences in protein synthesis between the *tif51A-1* mutant and the wild-type strain at restrictive temperature for the nLuc reporter alone, which targets the cytosol (Fig. 2 D). However, the synthesis of Cyc1, Cox5a, and Sdh2 luciferase

fusions was significantly affected at restrictive temperatures in the *tif51A-1* strain (Fig. 2 D).

Altogether, the obtained results point toward a specific mechanism connected to eIF5A to coordinately reduce the synthesis of mitoproteins at the translation level and, therefore, mitochondrial protein levels. However, this mechanism seems to not be connected to the presence of peptides requiring eIF5A for their synthesis during translation as none of the investigated mitochondrial mRNAs encode for polyprolines nor a high number of other eIF5A-dependent motifs.

eIF5A depletion induces the mitochondrial protein import stress mitoCPR and MitoStores

The "drug membrane transport" functional group, which includes the ATP-binding cassette (ABC) transporters Pdr5, Snq2, and Yor1, was found among the few GOs upregulated in the eIF5A mutant in our proteomic study (Fig. 1 A and Fig. S1 D and proteomic DATA). The evolutionarily conserved transporter *PDR5* has been shown to be induced during the mitochondrial stress response called the mitochondrial compromised protein import response (mitoCPR) (Weidberg and Amon, 2018). mitoCPR is induced upon defects in the translocation and import of mitoproteins to increase the activity of the proteasome in the cytosol, remove accumulated precursors from the TOM complex, and stabilize homeostasis. This response relies on the Pdr3-mediated transcriptional activation of different genes related to the multidrug resistance response, such as *PDR5*, which is involved in lipid metabolism and transport. The Pdr3-induced expression of Cis1, among others, recruits the AAA-protease Msp1 to the TOM translocase of the MOM to mediate the removal of accumulated mitoproteins upon import failure (Weidberg and Amon, 2018). To investigate if the mitoCPR response was induced upon eIF5A depletion, we analyzed the mRNA expression of *PDR3* and the Pdr3-responsive genes *MPS1*, *GRE2*, *PDR1*, *PDR3*, *PDR5*, *PDR15*, and *CIS1* in the *tif51A-1* mutant at restrictive temperature. The *tif51A-1* mutant, but not the wild-type, showed a significant upregulation of all genes except *MSP1*, with *CIS1* and *PDR5* the most induced mRNAs (Fig. 3 A).

When induced by Pdr3, the Pdr5 ABC membrane transporter is observed in the plasmatic membrane, where it mediates the efflux of xenobiotics, as well as in the vacuole, where it is degraded (Sarkadi et al., 2006). We fused the Pdr5 ORF to GFP and analyzed its cellular localization by fluorescence microscopy. We found that the levels of Pdr5 were almost non-detectable in the wild-type strain at both temperatures as well as in the *tif51A-1* strain at permissive temperature. However, at restrictive temperatures, Pdr5 protein levels were significantly induced in the *tif51A-1* strain and could be observed at their expected cellular locations (Fig. 3, B and C). Then, we added Nile Red, a Pdr5-specific substrate that stains lipid granules, to the cell cultures. We observed a red fluorescent signal inside the cells in all the tested conditions except for the *tif51A-1* mutant at restrictive temperature, indicating that high Pdr5 pumping activity excludes the Nile Red from these cells (Fig. S3, A and B).

Along with a transcriptional response, it has been found that mitoproteins can aggregate in the cytosol upon induction of mitochondrial import stress (Nowicka et al., 2021; Krämer et al., 2023). To explore the potential mislocalization of mitoproteins targeted to different locations within the mitochondria following eIF5A depletion, we investigated their distribution relative to a Su9-mCherry marker, which served to visualize the overall mitochondrial network. Tom70 is part of the TOM complex, placed in the MOM. Cytochrome c isoform 1 (Cyc1) is involved in the transfer of electrons during cellular respiration and targets the IMS. Yta12 is an m-AAA protease component required for the degradation of misfolded or unassembled proteins and targets the MIM. Ilv2 is an acetolactate synthase involved in the synthesis of isoleucine and valine and targets the MM. We found that the outer membrane protein Tom70 shows no difference between the wild-type and *tif51A-1* mutant at permissive and restrictive temperatures (Fig. 3 D and Fig. S3 C). Fig. 3, E–G show that at restrictive temperatures Yta12, Cyc1, and Ilv2 are localized in the mitochondria in the wild-type strain but, in the *tif51A-1* mutant, they also form foci, which do not co-localize to the mitochondria. On the contrary, no foci were observed at permissive temperatures (Fig. S3, D–F). Although Ilv2 has been described to accumulate as one big aggregate in the nucleus upon protein import failure (Shakya et al., 2021), we found that in the absence of eIF5A, this protein accumulates in multiple and distributed foci, similarly to the mislocalized protein aggregates of Cyc1 and Yta12.

Next, we asked about the intracellular localization and composition of these eIF5A-dependent mitoprotein foci. Different cellular destinations for mitoprotein aggregates have been described including the cytosol, endoplasmic reticulum, and nucleus (Shakya et al., 2021). DAPI staining of the nucleus of the cells indicated that Cyc1 aggregates were not co-localizing in the nucleus and thus seemed to be part of the cytosol (Fig. 3 H). To gain insight into the accumulation of non-imported mitochondrial precursors in cytosolic granules upon eIF5A depletion, we investigated whether chaperones such Hsp104 could be controlling this process. Hsp104 is a disaggregase that binds to aggregated or misfolded proteins and disentangles them in an ATP-dependent manner (Sanchez and Lindquist, 1990; Gates et al., 2017; Hill et al., 2017). Recently, it was found that induction of mitochondrial import stress can cause cytosolic accumulation and co-localization of MM-destined precursor proteins with Hsp104 granules. We fused Hsp104 ORF to RFP in a strain already expressing Cyc1-GFP and analyzed its cellular localization. We found that a high percentage (>80%) of Hsp104 foci co-localize with Cyc1 aggregates (Fig. 3 I and Fig. S4 H).

Altogether, these results suggest that depletion of eIF5A compromises mitochondrial protein import as the induction of the Pdr3-mediated mitoCPR response and the cytosolic Hsp104 aggregation of precursor mitoproteins into MitoStores have been described as mechanisms to reduce toxicity from accumulated mitoprotein precursors and to restore cellular homeostasis upon import failure.

eIF5A alleviates ribosome stalling of *TIM50* mRNA encoding the co-translationally imported MIM receptor

Given the elevated mitochondrial protein import stress response found upon eIF5A depletion, we sought to explore the mechanism by which eIF5A impacts mitochondrial protein import.

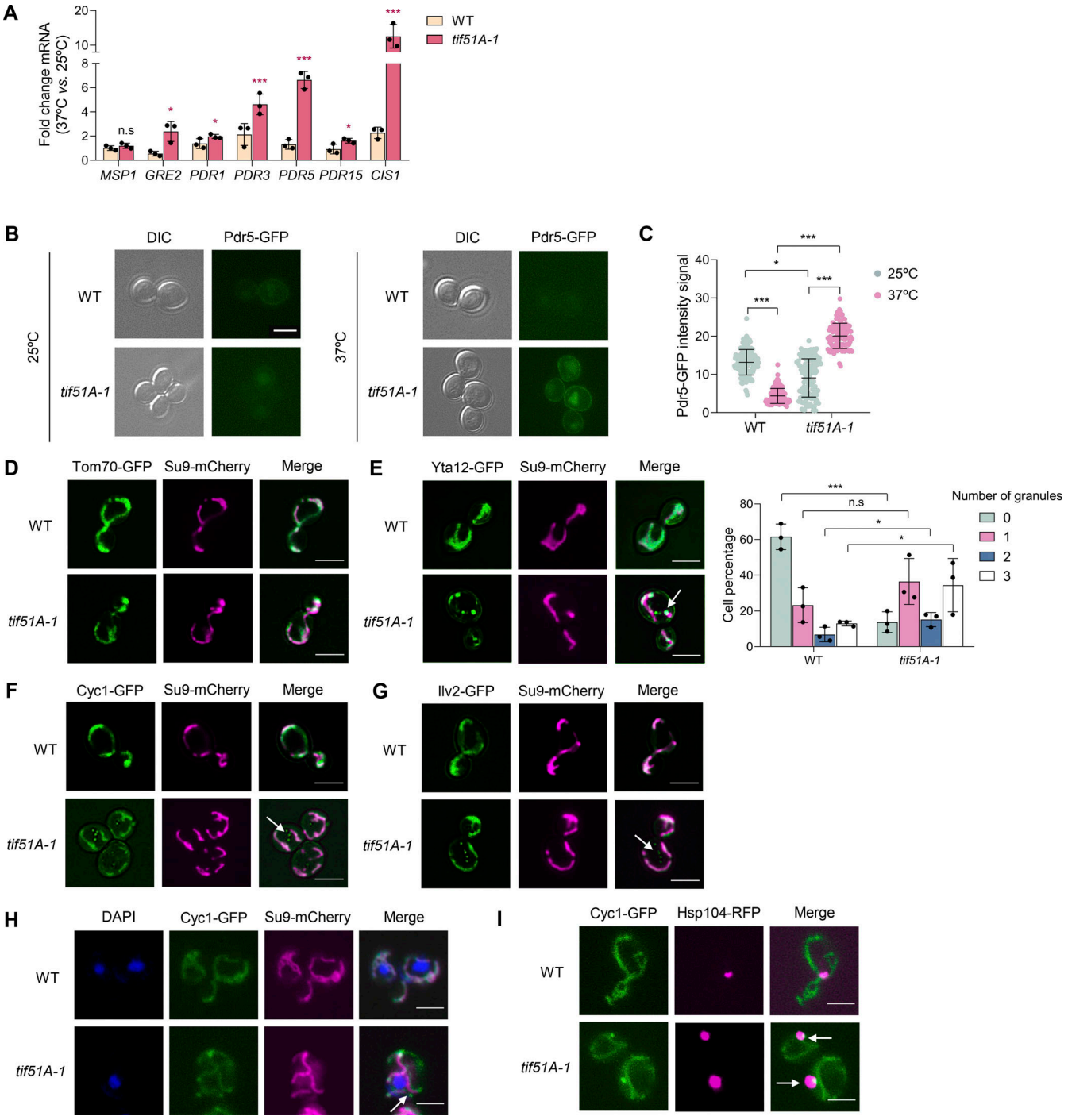

Figure 3. **eIF5A deficiency generates mitoCPR stress and mislocalization of mitoproteins. (A)** Wild-type strain and *tif51A-1* were cultured in SGal medium at 25°C until reaching post-diauxic phase and then transferred to 25°C or 37°C for 4 h. mRNA relative levels from mitoCPR genes were determined by RT-qPCR. **(B)** Wild-type strain and *tif51A-1* expressing Pdr5-GFP were cultured as in A and then subjected to fluorescence microscopy. **(C)** Quantification of Pdr5-GFP fluorescent signal from at least 150 cells. **(D–G)** Wild-type strain and *tif51A-1* expressing Tom70-GFP (D), Yta12-GFP (E), Cyc1-GFP (F), or Ilv2-GFP (G) and Su9-mCherry were cultured as in A and subjected to fluorescence microscopy. Scale bar, 4 µm. **(E)** Quantification of cells with Yta12 aggregates at 37°C is shown (right). **(H)** Wild-type strain and *tif51A-1* expressing Cyc1-GFP and Su9-mCherry were cultured as in A and incubated for 30 min with DAPI prior microscopy to stain the nuclei. Scale bar, 4 µm. **(I)** Wild-type strain and *tif51A-1* expressing Cyc1-GFP and Hsp104-RFP were cultured as in A and subjected to fluorescence microscopy. Scale bar, 4 µm. **(B and D–I)** A representative image is shown from three independent experiments. Arrows in E–H indicate mitoprotein cytosolic aggregates. Data information: In A, C, and E, results are presented as mean ± SD from three independent experiments. The statistical significance was measured by using a two-tailed paired Student's *t* test. *P < 0.05, ***P < 0.001. n.s means no significant differences.

Tim50 protein is a receptor component of the MIM translocase complex TIM23, which recognizes the N-terminal MTS-containing proteins after emerging from the TOM complex and mediates their import to the mitochondrial inner membrane and matrix (Mokranjac and Neupert, 2009; see review Chaudhuri et al., 2021). Interestingly, Tim50 contains 10 proline residues in a 14-amino acid region in the first half of the protein with 7 of them consecutive (Fig. 4 A) and, therefore, is a proposed putative eIF5A target (Barba-Aliaga and Alepuz, 2022b). This region is quite conserved across different yeast species (Fig. S4 A). In addition, *TIM50* overexpression has previously been found to induce mitochondrial protein import defects (Weidberg and Amon, 2018). We therefore sought to investigate the possible role of eIF5A in *TIM50* mRNA translation. First, we genomically attached an HA tag to Tim50 to quantify the impact of eIF5A depletion on endogenous Tim50 expression. We found a significant drop in Tim50 protein levels upon eIF5A depletion with no decrease in its mRNA levels (Fig. S4 B). Moreover, expressing a *FLAG-TIM50-GFP* version under a *GAL*-inducible system, we detected a reduction in Tim50 protein synthesis in the two eIF5A mutants, which was not due to lower levels of the corresponding mRNA, further suggesting a role of eIF5A in the translation of *TIM50* mRNA (Fig. S4 C).

Tim50 protein half-life is ∼9.6 h (Christiano et al., 2014), which makes it more difficult to measure large differences in new protein synthesis. Therefore, to accurately test and quantify the eIF5A-dependency for *TIM50* mRNA translation, we fused two different versions of the *TIM50* DNA sequence to a $TetO_7$-inducible nLuc reporter: the first one expressing the wild-type *TIM50* sequence and the second one expressing *TIM50* with a deletion of the seven consecutive prolines (Tim50Δ7Pro) (Fig. 4 B). After inducing expression, we analyzed the protein synthesis by incubating for 1 h in anhydrotetracycline-supplemented media the wild-type and mutant cells. After analyzing the protein synthesis, it was observed that the *tif51A-1* mutant showed a threefold reduction in the synthesis of Tim50 at restrictive temperature compared with the wild-type strain, further suggesting Tim50 as an eIF5A target for translation elongation (Fig. 4 C). Considering that final protein abundance is determined by both mRNA levels and translation, we confirmed that the lower protein levels were not attributed to *TIM50* transcription since the mRNA levels were even slightly higher in the *tif51A-1* mutant at restrictive temperature compared with wild-type (Fig. S4 D). To test if the decrease in protein synthesis was due to the presence of a high number of prolines in the Tim50 sequence, we analyzed the Tim50 version containing deletions of the seven consecutive prolines. Results indicated that after removing the proline-rich region of Tim50, protein synthesis was rescued in the *tif51A-1* mutant at 37°C and reached similar protein levels in the wild-type strain (Fig. 4 D).

Inducible reporter assays enabled us to calculate both the overall expression levels as well as the time needed for translation elongation through the region upstream of the nLuc reporter gene (Masser et al., 2016; Hou et al., 2023). By using the Schleif plotting technique (Schleif et al., 1973; Zhu et al., 2016), we compared the amount of time needed to detect luciferase signal from a reporter only expressing nLuc and the two Tim50 reporters. Then, we obtained the time required for ribosomes to translate each of the Tim50 versions. We found that the time required for translating a wild-type *TIM50* mRNA was significantly increased in the *tif51A-1* mutant at restrictive temperature. If a cell needs ∼2 min to generate one full Tim50 polypeptide, upon eIF5A depletion the ribosomes need almost 4 min to achieve the complete translation of this mRNA. However, the synthesis time required for translating *TIM50Δ7Pro* mRNAs was almost identical to that in the corresponding wild-type strain (Fig. 4 E). This extended translation duration was indicative of a ribosome stall at the polyprolines. To further confirm ribosome stalling, we analyzed the ribosome density across the *TIM50* transcript in control and an eIF5A degron strain (Schuller et al., 2017). We found a precipitous drop-off in ribosome density exactly where the stretch of polyprolines is located in Tim50 (540–561 bp) upon eIF5A depletion but not in the control strain (Fig. 4 F and Table S6). Furthermore, we found an increased accumulation of ribosome density ∼300 bps upstream of the polyproline stretch upon eIF5A depletion. As ribosomes can protect ∼30 bp of mRNA, this points to potentially up to 10 ribosomes in a traffic jam upstream of the polyproline stretch. The absence of ribosomes after the stretch of polyprolines is further evidence of ribosome stalling and the induction of ribosome quality control (RQC) at the polyproline residues. Together, these results indicated that Tim50 downregulation in the *tif51A-1* mutant was due to a decrease in translation because ribosomes stalled along the proline-rich region of its sequence.

We extended our bioinformatic analysis of ribosome distribution changes to further investigate whether eIF5A depletion affects other nuclear-encoded, co-translationally localized mitochondrial mRNAs. We found similar pronounced shifts in ribosome distribution in several examples including Yta12, an inner membrane AAA protease, and Mss51, a mitochondrial translational regulator (Fig. S4 E and Table S6). In both cases, we observed a surge of ribosomes at proline-rich regions, followed by a marked decrease in ribosome density. This pattern leads to a significant drop in ribosome coverage from the 5′ to the 3′ end of these mRNAs. However, as *TIM50* mRNA stands out due to its high expression level and the most pronounced changes in polarity and ribosome dropoff (Table S6), we chose to further characterize the *TIM50* mRNA in our subsequent analyses.

TIM50 mRNA is constitutively localized to the vicinity of the mitochondrial surface and the import of Tim50 protein to mitochondria occurs co-translationally (Williams et al., 2014; Tsuboi et al., 2020). To confirm that ribosome stalling along *TIM50* mRNA upon eIF5A depletion was mitochondrially localized, we visualized mitochondria using the marker Su9-mCherry and *TIM50* mRNAs with the MS2 tag system (Tsuboi et al., 2020) in both wild-type and *tif51A-1* strains at restrictive temperature. We observed *TIM50* mRNA to be strongly associated with the mitochondrial surface in both strains (Fig. S4 F), confirming that Tim50 ribosome stalling occurs adjacent to the mitochondrial surface.

Finally, we asked if ribosome stalling along *TIM50* mRNA upon eIF5A depletion could affect its protein localization. We observed that Tim50 strongly localizes to the mitochondria in the wild-type strain. However, we found the presence of Tim50 foci which do not co-localize to the mitochondria in the *tif51A-1*

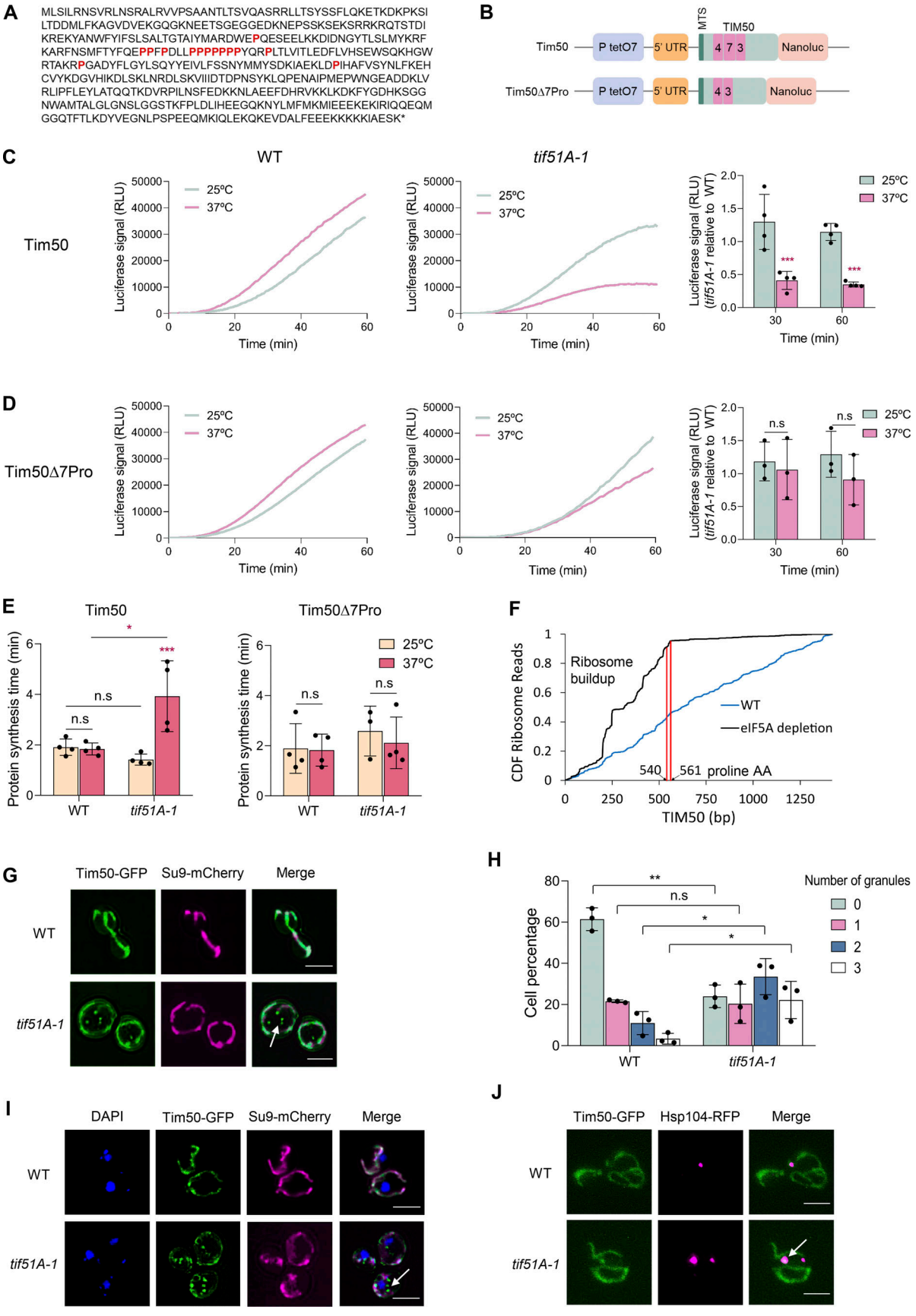

Figure 4. **eIF5A depletion causes *TIM50* polyproline ribosome stalling, decreased Tim50 protein levels, and mislocalization. (A)** Scheme showing Tim50 protein sequence. Proline amino acids (P) in the proline-rich region are typed in red color. **(B)** Scheme showing the two different nLuc versions used in

this study. Proline numbers are shown in magenta. **(C and D)** Wild-type strain (left) and *tif51A-1* (middle) expressing the wild-type Tim50 (C) or Tim50Δ7Pro (D) were cultured in YPD until early exponential phase and then transferred to 25°C or 37°C for 4 h. After the addition of doxycycline to induce luciferase expression, the luminescence levels generated by nLuc after the addition of the furimazine substrate were measured along time (expressed as relative luciferase units, RLU). A representative experiment is shown. Quantification of the Tim50 protein levels is shown on the right. **(E)** Full protein synthesis time was calculated for wild-type strain and *tif51A-1* expressing the wild-type Tim50 (left) or Tim50Δ7Pro (right). **(F)** Fraction of ribosome reads of various lengths along *TIM50* transcript in Schuller et al. (2017) ribosome profiling libraries. **(G)** Wild-type strain and *tif51A-1* expressing Tim50-GFP and Su9-mCherry were cultured in SGal medium at 25°C until reaching post-diauxic phase, transferred to 37°C for 4 h, and subjected to fluorescence microscopy. **(H)** Quantification of cells with Tim50 aggregates at 37°C is shown. **(I)** Wild-type strain and *tif51A-1* expressing Tim50-GFP and Su9-mCherry were cultured as in G and incubated for 30 min with DAPI prior microscopy to stain the nuclei. **(J)** Wild-type strain and *tif51A-1* expressing Tim50-GFP and Hsp104-RFP were cultured as in G. **(G, I, and J)** A representative image is shown from three independent experiments. Arrows indicate Tim50 cytosolic aggregates. Scale bar, 4 µm. Data information: In C–E and H Results are presented as mean ± SD from at least three independent experiments. The statistical significance was measured by using a two-tailed paired Student's *t* test. *P < 0.05, **P < 0.01, ***P < 0.001. The asterisks located above the columns of the graph represent a comparison between temperatures within the same strain. The asterisks found at the top of the bars additionally indicate comparisons between the indicated strains at the same treatment condition. n.s means no significant differences.

mutant at restrictive temperature whereas no aggregates were observed at permissive temperature (Fig. 4 G and Fig. S4 G). The number of cells containing more than one of these Tim50 aggregates was found to be significantly increased in the *tif51A-1* mutant at restrictive temperatures (Fig. 4 H). DAPI staining of the nucleus of the cells indicated that Tim50 aggregates were not co-localizing in the nucleus, and thus, seemed to be part of the cytosol (Fig. 4 I). To gain insight into the accumulation of Tim50 into MitoStores, as previously seen for Cyc1, we fused Hsp104 ORF to RFP in a strain already expressing Tim50-GFP and found that a high percentage (>70%) of Hsp104 foci co-localize with Tim50 aggregates (Fig. 4 J and Fig. S4 H). Thus, these data strongly suggest that *TIM50* mRNA translation is directly dependent on eIF5A, and its deficiency generates ribosome stalling on the mitochondrial surface and precursor protein accumulation in the cytosol.

Deletion of Tim50 proline stretch in eIF5A mutant restores mitochondrial protein import without rescuing mitochondrial respiration

Herein, we have demonstrated how upon eIF5A depletion, Tim50 translation occurring at the mitochondrial surface stalls in the polyproline stretch and its protein synthesis is decreased. This seems to generate specific import defects for mitoproteins, which accumulate and aggregate in the cytosol. Therefore, we asked if a reduction in Tim50 stalling and rescuing of Tim50 protein levels would alleviate the import collapse and its derived effects associated with eIF5A loss of function. To test this, we generated two strains expressing the endogenous Tim50 protein without the region containing the seven consecutive prolines of its sequence (Tim50ΔPro) fused to GFP: the first one in a wild-type (BY4741) background and the second one in a *tif51A-1* mutant background. In these strains, the endogenous *TIM50* gene is mutated so that the only source of Tim50 protein for the cell is the eIF5A-independent version Tim50ΔPro. Here, translational stalling of *TIM50* mRNA occurring at the mitochondrial surface is no longer present and Tim50 reporter levels are rescued upon eIF5A depletion (Fig. 4, C–E). We confirmed that Tim50ΔPro protein had similar stability and expression levels to the native Tim50 version in both wild-type and *tif51A-1* cells (Fig. S5, A and B). Surprisingly, the functionality of the Tim50ΔPro version was shown to be almost unaffected. We observed no obvious growth differences in glycerol media between the wild-type strain containing full Tim50 or Tim50ΔPro (Fig. 5 A), although the proline-rich region is found in the presequence-binding groove of the Tim50 IMS domain, which functions in receiving the proteins in the TIM23 complex (Li and Sha, 2015). Therefore, the proline-rich region is not essential for cell viability under the respiratory conditions tested and thus, for the proper mitochondrial import.

We then tested the effect of substituting the endogenous Tim50 by Tim50ΔPro, whose translation is eIF5A-independent, on mitochondrial function and growth on respiratory media in eIF5A mutant cells. Expression of Tim50ΔPro did not rescue the growth of the *tif51A-1* mutant under glycerol at semipermissive temperature (Fig. 5 A). This result points to the idea that impaired *TIM50* translation is not the only mechanism linking eIF5A to mitochondrial function. In addition, when we checked the accumulation of the membrane potential-dependent dye mitotracker red, we observed a slight increase in the membrane potential at permissive and restrictive temperatures in the *tif51A-1* Tim50ΔPro mutant respect to *tif51A-1* mutant cells expressing wild-type Tim50 (Fig. 5, B and C).

We next tested whether rescue of Tim50 translational stalling and protein levels would rescue the mitochondrial import phenotypes we observed in the eIF5A depletion. We found a reduction in Tim50 cytosolic protein aggregates upon removal of the stretch of prolines, indicating proper protein import (Fig. 5, D and E). Furthermore, we found that the mRNA levels of the most induced mitoCPR genes (*PDR3*, *PDR5*, and *CIS1*) were significantly decreased in the *tif51A-1* Tim50ΔPro mutant (Fig. 5 F).

Ribosome stalling at *TIM50* mRNA is the main cause of the mitochondrial stress response and mitoprotein translation downregulation upon eIF5A depletion

The previous results with Tim50ΔPro align with the reversal of the mitochondrial import phenotypes induced by eIF5A depletion. This reversal may result from either the restoration of Tim50 protein levels or the alleviation of ribosome stalling along *TIM50* mRNA, which localizes at the mitochondrial surface to allow the co-translational import of Tim50 protein. To try to distinguish between these two possibilities, we constructed new wild-type and *tif51A-1* mutant yeast strains containing both, the eIF5A-independent *TIM50ΔPro* copy and a second wild-type copy of the *TIM50* gene.

In the new eIF5A mutant strain expressing these two copies, Tim50 protein levels were restored by expression of the

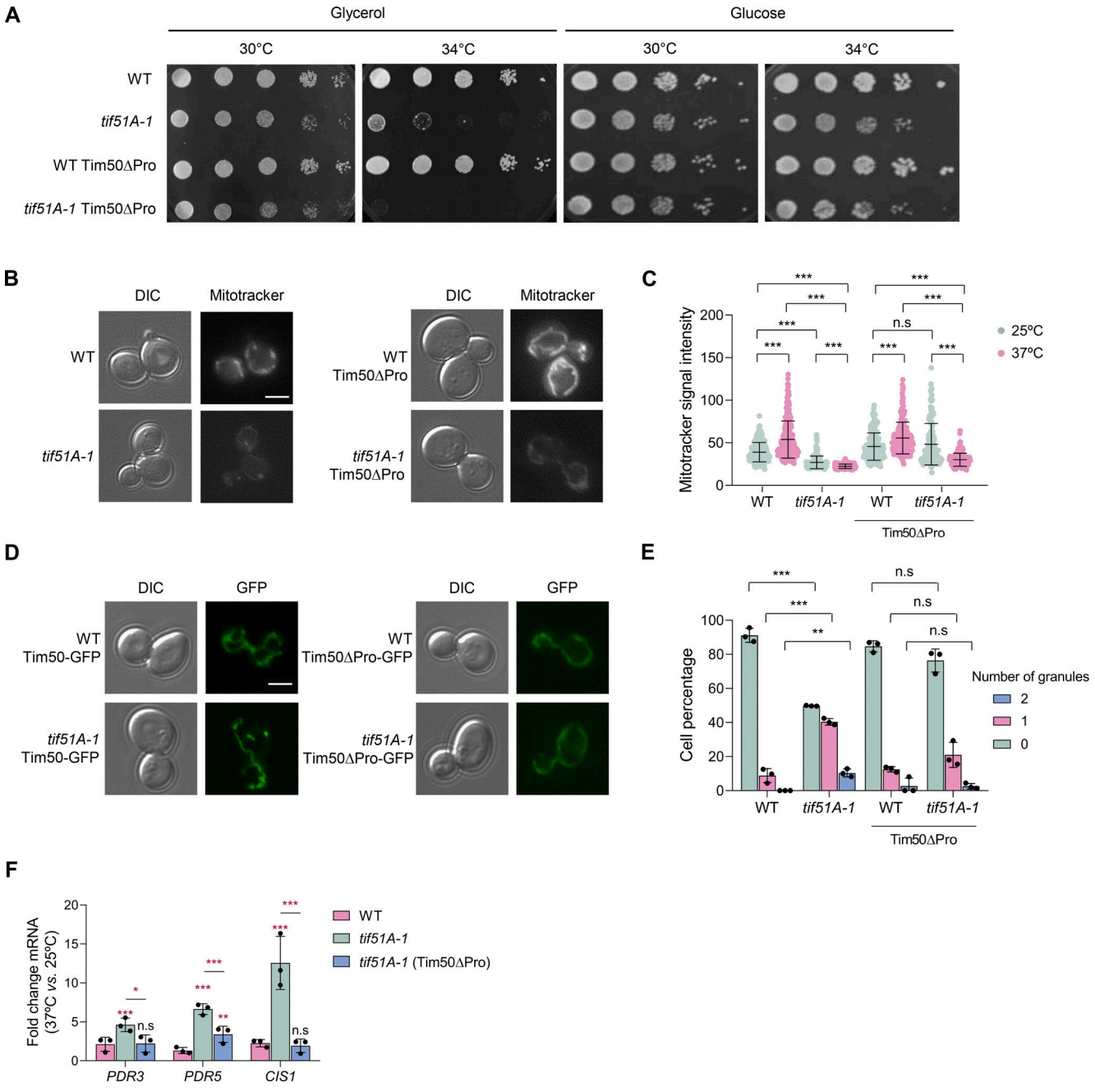

Figure 5. **Deletion of the Tim50 polyproline stretch in the eIF5A mutant does not rescue mitochondrial respiration but cancels the mitoCPR response induction. (A)** Growth of the wild-type, *tif51A-1*, wild-type Tim50ΔPro, and *tif51A-1* Tim50ΔPro was tested in YPGly and YPD media at the indicated temperatures. **(B–E)** Wild-type, *tif51A-1*, wild-type Tim50ΔPro, and *tif51A-1* Tim50ΔPro were cultured in SGal medium until reaching post-diauxic phase at 25°C, transferred to 37°C for 4 h, and subjected to fluorescence microscopy. A representative image from three independent experiments is shown. Scale bar, 4 µm (B and D). Cells were incubated for 30 min with Mitotracker prior to microscopy to quantify the mitochondrial membrane potential (B). Quantification of Mitotracker fluorescent signal from at least 150 cells (C). Quantification of cells presenting 0, 1, or 2 Tim50 aggregates at 37°C is shown (E). **(F)** Wild-type, *tif51A-1*, and *tif51A-1* carrying Tim50ΔPro were cultured as in B. mRNA relative levels from mitoCPR genes were determined by RT-qPCR. Data information: In C, E, and F, results are presented as mean ± SD from three independent experiments. The statistical significance was measured by using a two-tailed Student's *t* test. *P < 0.05, **P < 0.001, ***P < 0.001. n.s means no significant differences.

Tim50ΔPro protein version (Fig. 4, D and E; and Fig. S5 B), while eIF5A depletion generates ribosome stalling at the wild-type *TIM50* mRNA encoding the polyproline stretches (Fig. 6 A). First, we confirmed that both *TIM50* and *TIM50ΔPro* mRNAs had similar levels in wild-type and *tif51A-1* strains (Fig. S5 C). Using both qPCR of the endogenous *PDR5* mRNA and an integrated *PDR5* promoter-driven nLuc reporter, we examined mitoCPR stress induction. We found that, at restrictive temperature, the restoration of low Pdr5 mRNA and protein observed in the *tif51A-1* strain containing Tim50ΔPro as the sole source of Tim50

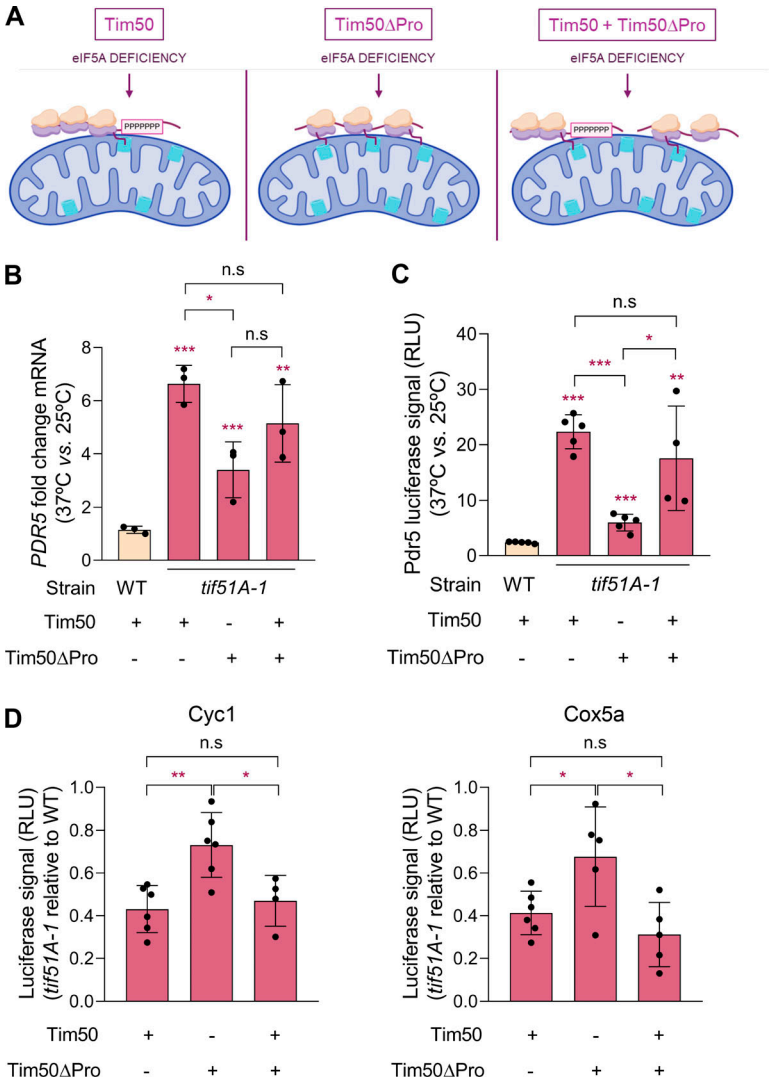

Figure 6. **Ribosome stalling along *TIM50* mRNA under eIF5A deficiency favors translation downregulation of mitoproteins. (A)** Scheme showing ribosome stalling along *TIM50* mRNA and Tim50 translocase receptor protein levels (in blue) when expressing different versions of *TIM50*. P indicates a proline-encoding codon. The figure was processed using BioRender (RRID:SCR_018361). **(B)** Wild-type and *tif51A-1* strains expressing Tim50, Tim50ΔPro or both were cultured in SGal medium until reaching post-diauxic phase at 25°C and transferred to 37°C for 4 h. mRNA relative levels from *PDR5* were determined by RT-qPCR. **(C)** Wild-type and *tif51A-1* strains harboring Tim50, Tim50ΔPro, or both and expressing PDR5p-nLuc were cultured in YPD until the early exponential phase and then transferred to 25°C or 37°C for 4 h. The luminescence levels generated by the nLuc after the addition of the furimazine substrate were measured along time and the protein was quantified after 10 min. **(D)** Wild-type and *tif51A-1* strains harboring Tim50, Tim50ΔPro, or both and expressing Cyc1-nLuc (left) or Cox5a-nLuc (right) were cultured as in C. Luminescence levels were measured as in C. Data information: In B–D, results are presented as mean ± SD from three independent experiments. The statistical significance was measured by using a two-tailed Student's *t* test. *P < 0.05, **P < 0.001, ***P < 0.001. The asterisks located above the columns of the graph represent a comparison relative to the wild-type strain. The asterisks found at the top of the bars additionally indicate comparisons between the different Tim50 versions within the same strain. n.s means no significant differences.

was changed to a higher *PDR5* expression when a second copy of wild-type *TIM50* was also expressed (Fig. 6, B and C). Therefore, the expression of *PDR5* was found to be comparable between the two *tif51A-1* strains, one containing the Tim50 wild-type and the other containing an additional Tim50ΔPro. This suggests that the effect of eIF5A mutation on the Tim50 wild-type copy is phenotypically dominant. We next tested how the expression of single Tim50ΔPro or double Tim50ΔPro plus Tim50 could affect the translation of OXPHOS reporters in cells upon eIF5A depletion. When the translational stalling along *TIM50* was rescued by removing the prolines (cells expressing Tim50ΔPro), we observed a partial but significant rescue of the synthesis of Cyc1 and Cox5A reporters upon eIF5A depletion. However, the addition of a second *TIM50* copy was not able to rescue the reduced protein synthesis of Cyc1 and Cox5A (Fig. 6 D). Taken together, these results suggest that the translational defects observed upon eIF5A depletion are secondary effects driven by mitochondrial import stress and that the ribosome stalling at *TIM50* mRNA is sufficient to cause both effects and is, therefore, a primary cause of the mitochondrial import defects upon eIF5A depletion.

Discussion

In this study, we have expanded our knowledge on the effects of eIF5A depletion on mitochondrial function and identified one of the possible molecular mechanisms by which eIF5A is required to maintain mitochondrial activity. We have shown that eIF5A is needed to alleviate ribosome stalling along the *TIM50* mRNA on the mitochondrial surface as it is being co-translationally imported and thus impacts mitochondrial import. Upon eIF5A depletion, the mitochondrial import of many inner mitoproteins is compromised. We have seen that non-imported mitoproteins aggregate in the cytosol as a consequence of the import stress response provoked by the lack of eIF5A. A response for the clearance of stalled proteins in the mitochondrial surface has been shown to be mediated by the mitoCPR response, which induces, through the transcription factor Pdr3, the coordinated action of Cis1 and Msp1 to promote the degradation of arrested precursor proteins (Weidberg and Amon, 2018). Altogether, our results demonstrate that low levels of eIF5A cause mitochondrial stress by inducing *TIM50* ribosome stalling and reducing Tim50 expression (Fig. 7).

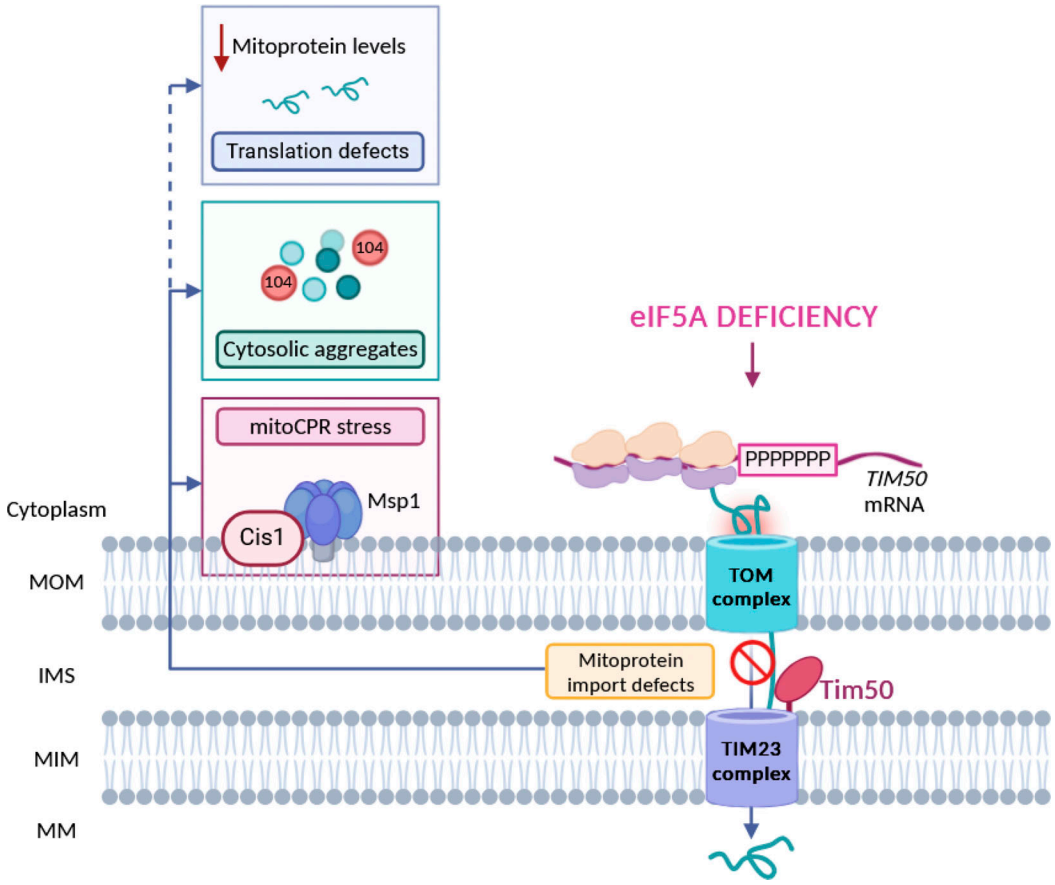

Figure 7. **Model for the eIF5A-mediated regulation of the mitochondrial function.** Upon eIF5A depletion, ribosomes translating *TIM50* mRNA to synthesize the Tim50 proline-rich region (PPPPPPP) become stalled and, thus, the mitochondrial import of co-translationally inserted proteins targeting the IMS, MIM, and MM is compromised. The non-imported mitochondrial precursors start aggregating in the cytosol bound to chaperone Hsp104. Then, the mitoCPR response is induced to clear the proteins accumulating in the mitochondrial surface through the action of Cis1 and Msp1. In addition, the lack of eIF5A reduces the translation of many RNAs encoding mitoproteins so the levels of most mitochondrial proteins become reduced. Figure was processed using BioRender (RRID:SCR_018361).

Our results also indicate that the accumulation of non-imported precursors in specific deposits in the cytosol is buffered by cytosolic chaperones, mainly Hsp104, to relieve the proteotoxic stress. These results are in line with the recent description of the cytosol as a place with the capacity to store mitochondrial precursor proteins in dedicated storage granules that are controlled by the cytosolic chaperone system, with Hsp104 binding the N-terminal presequences of mitoproteins (Krämer et al., 2023). Similarly, the observed Pdr5 induction upon eIF5A depletion seems indicative of a cellular detoxification effort to eliminate toxic substrates accumulating in the cytosol in the context of protein aggregates accumulation.

Upon prolonged mitochondrial dysfunction, the stress response is usually accompanied by cytosolic translation attenuation to reduce the synthesis of precursors and the protein load to translocases. The general translation is known to be downregulated upon treatment with multiple mitochondrial stressors such as defective mitochondrial biogenesis (Wrobel et al., 2015), clogger expression (Boos et al., 2019), oxidative stress (Topf et al., 2018), and mitochondrial depolarization with high carbonyl cyanide *m*-chlorophenyl hydrazone (CCCP) doses (Schäfer et al., 2022). Herein, we have found that eIF5A depletion specifically downregulates the expression of most mitoproteins. The reduction in the number of ribosomes bound to mitoprotein mRNAs could be interpreted as a specific translational downregulation but also as a result of ribosome stalls at the 5′ ORF regions, where MTSs are found (Table S6). We observed that while general cytosolic translation remained unaffected, the translation of proteins targeting the mitochondria was found to be uniformly affected, suggesting a connection between the import status and the translation of mitoproteins that need to be translocated. In the last years, it has been proposed that eIF5A is necessary for the translation of specific mitoproteins with that specificity residing in the amino acid sequences at their N-terminal/MTS sequences, especially those ones with weak interactions with the peptide exit tunnel, yet it was unclear if this was a direct effect (Puleston et al., 2019; Zhang et al., 2022). The fact that Tim50ΔPro partially alleviated the translational repression of Cyc1 and Cox5A even upon eIF5A depletion suggests that some aspects of this translational regulation may result indirectly from eIF5A depletion. This could potentially be linked to the mitochondrial import stress generated rather than being directly regulated by eIF5A. Furthermore, the translational repression of Cyc1 and Cox5A and the induction of Pdr5 caused by

the addition of a second copy of *TIM50* in the eIF5A mutant containing *TIM50ΔPro* suggests that ribosome stalling along the *TIM50* mRNA at the mitochondrial surface is the primary cause of the mitochondrial import defects. Nevertheless, more work will be needed to further decipher the specific molecular changes linking eIF5A, the general translation of mitochondrial proteins, and overall mitochondrial function.

The presented results herein highlight the idea that multiple mechanisms, besides Tim50 regulation, link eIF5A to the mitochondrial function. While we found the recovery of Tim50 function with the Tim50ΔPro to partially rescue the mitochondrial import stress response after 4 h of eIF5A depletion, this was not sufficient to fully recover the MIM potential nor to rescue the growth on respiratory media for longer times at semipermissive temperatures. This could be explained by the fact that over sustained periods at semipermissive temperatures, eIF5A becomes further depleted and causes other mitochondrial mRNAs that are less sensitive to eIF5A levels to become stalled and drive similar mitochondrial stress responses. Indeed, ribosome profiling data from Schuller et al. (2017) show that other co-translationally inserted mRNAs encoding proline stretches (such as the Yta12 and Mss51 mRNAs) have ribosome distributions similar to Tim50 (Fig. S4 E and Table S6). Upon eIF5A degradation, there is an increase in ribosome density right before the corresponding proline region while a decrease in density becomes visible right after it, suggesting the induction of RQC mechanisms. Therefore, it is of interest to explore other putative mitochondrial targets with eIF5A-dependent motifs in their sequences and conserved in higher eukaryotes, as they could underlie the long-term mitochondrial defects that are still observed even when Tim50 protein levels are rescued.

In this regard, could translational stalling of co-translationally imported mitoproteins underlie the mitochondrial defects found upon eIF5A depletion in mammalian cells? While Tim50 polyproline region is highly conserved across different yeast species, including the pathogenic fungi *Candida albicans* (Fig. S4 A), human Tim50 sequence contains 27 prolines, but these are scattered throughout the sequence rather than clustered in a specific region as in *S. cerevisiae*'s. However, several other eIF5A-dependent motifs are found in the amino acid sequences of the human homologs of Tim50, Yta12, and Mss51 that could potentially generate ribosome stalling in their mRNAs upon eIF5A depletion as observed in yeast (Table S6). Intriguingly, it was recently found that mutant Huntingtin protein, which is associated with decreased mitochondrial activity, drives eIF5A depletion and pervasive ribosome stalling (Aviner et al., 2024). Furthermore, clogging of translocases and cytosolic deposition of mitochondrial precursors have been implicated with some neurodegenerative disorders. Aggregation of mitoproteins in the cytosol increases misfolding of α-synuclein and amyloid precursor proteins, which are involved in Parkinson's and Alzheimer's diseases, as they can co-aggregate together, engage translocases, and further increase the clogging hazard (Cenini et al., 2016; Nowicka et al., 2021). Importantly, data shown herein points to a novel and more likely mitochondrial stress generated by lack or defects in eIF5A protein that could be found in nature and raised as one of the underlying causes of impaired protein uptake in disease contexts. Thereby, eIF5A and its well-characterized hypusination precursor spermidine could be considered potential candidates to potentiate the activity of mitochondrial import machinery in compromised cells.

Materials and methods

Yeast strains, plasmids, and growth conditions

All *S. cerevisiae* strains and plasmids used herein are listed in Tables S2 and S3, respectively. *S. cerevisiae* cells were grown in either liquid YPD (1% yeast extract, 2% peptone, and 2% dextrose/glucose), YPGly (1% yeast extract, 2% peptone, and 2% glycerol), synthetic complete medium (SC) (2% glucose, 0.7% yeast nitrogen base [YNB], and Drop-Out complete [Kaiser, Formedium]) or SGal (2% galactose, 0.7% YNB, and Drop-Out complete).

For protein quantification and visualization under the microscope, a PCR-based genomic tagging technique was employed to tag the genomic full-length *COR1*, *IDH1*, *TIM50*, *TOM70*, *CYC1*, *YTA12*, *ILV2*, and *PDR5* ORFs with HA or GFP or the *HSP104* ORF with RFP. The plasmids pFA6a-3HA-HIS3MX, pFA6a-GFP-HIS3MX (Longtine et al., 1998), and pYM43-Redstar2-clonNAT were used as a template for PCR reaction using primers listed in Table S4. The resulting cassettes were transformed in the corresponding strains following the lithium acetate-based method (Gietz et al., 1992). All the integrations were confirmed by genomic DNA conventional PCR.

Plasmid pRS406-GPDp-Su9-mCherry-URA3 was integrated into the corresponding strains for expression of Su9 (subunit 9 of the F_0 ATPase) fused to mCherry and subsequent visualization of the mitochondrial network. To constitutively visualize *TIM50* single mRNAs, plasmids pRS405-CYC1p-MS2-4xGFP-LEU2 and plasmid pRS403-TIM50p-TIM50-flagiRFP-TIM50ter-MS2tag-HIS3MX (Tsuboi et al., 2020) were integrated in wild-type and *tif51A-1* strains.

Plasmid pGAL-FLAG-TIM50-GFP-URA3 was constructed from the plasmid pYES2-pGAL-FLAG-htt25QP-GFP-URA3 (Berglund et al., 2017). First, the yeast *TIM50* ORF was obtained by PCR using primers listed in Table S4. Then, plasmid pYES2-pGAL-FLAG-htt25QP-GFP-URA3 was linearized by restriction enzyme XagI (Cat# ER1301; Thermo Fisher Scientific) to replace *huntingtin* (*htt*) gene by *TIM50* gene by homologous recombination. The resulting plasmid was transformed in the corresponding strains, and transformants were selected in SC medium lacking uracil. To generate the strains harboring the deletion of the seven consecutive prolines from the *TIM50* gene sequence (Tim50ΔPro), the C-terminal TIM50-GFP sequence was amplified from the genomic DNA of the strain PAY1078 using primers listed in Table S4. The use of these primers resulted in the deletion of nucleotides 541–561 in *TIM50*, which encode for the seven prolines stretch of the Tim50 protein. The resulting PCR product was transformed in wild-type and *tif51A-1* strains as previously described. In addition, plasmid pRS305-TIM50-LEU was integrated into the corresponding strains harboring Tim50ΔPro for the expression of an extra copy of *TIM50*. All the integrations and deletions were confirmed by genomic DNA conventional PCR.

nLuc reporter constructs expressing different versions of the *TIM50* gene or other mitoproteins under the control of a

tetracycline-inducible operon ($tetO_7$) were generated by cloning the corresponding ORF in the plasmid ZP446, derived from pAG306 vector. ZP446 backbone was amplified by PCR using oligos listed in Table S4. The parental plasmid was digested by restriction enzyme DpnI (Cat#R0176S; New England Biolabs) and linearized plasmid was isolated by gel purification (Zymo Research). The ORF fragments for cloning were amplified by conventional PCR from wild-type genomic DNA using oligos listed in Table S4. After PCR product purification (Zymo Research), the fragments of interest were inserted into linearized ZP446 using Gibson Assembly. The resulting nLuc constructs were linearized by restriction enzyme NotI (Cat# #R3189; New England Biolabs) and integrated into the genome of the wild-type and *tif51A-1* cells by homologous recombination. All the Tim50-nLuc plasmids used in this study are listed in Table S3.

Experimental assays were performed with cells exponentially grown for at least four generations until the required OD_{600} at the corresponding temperature. Temperature-sensitive strains were grown at the permissive temperature of 25°C until the required OD_{600} and transferred to the non-permissive temperature of 37°C or 41°C for 4 h for complete depletion of eIF5A. For protein stability experiments described in the text, the media were supplemented with 100 µg/ml cycloheximide (CHX) (Cat# C7698; Sigma-Aldrich) for 5 h.

Proteomic analysis

For the proteomic analysis, three independent cultures of wild-type (BY4741), *tif51A-1*, and *tif51A-3* were grown exponentially in YPD at 25°C and then incubated at 41°C for 4 h. Proteins were extracted as previously described (Li et al., 2014) and analyzed in the SCSIE (Servei Central de Suport a la Investigació Experimental; Universitat de València). Protein samples (about 20 µg of protein) were digested with 500 ng of trypsin (Promega) and peptides were analyzed by an Ekspert nanoLC 42 nanoflow system (Eksigent Technologies, ABSCIEX) coupled to a nanoESI quadrupole-time of flight (qQTOF) mass spectrometry (6600plus TripleTOF, ABSCIEX). The tripleTOF was operated in SWATH mode. 5 µl of each sample were loaded onto a trap column (3 µm C18-CL 120 Ă, 350 µm × 0.5 mm; Eksigent) and desalted with 0.1% TFA at 5 µl/min for 5 min. The peptides were loaded onto an analytical column (3 µm C18-CL 120 Ă, 0.075 × 150 mm; Eksigent) equilibrated in 5% acetonitrile 0.1% FA (formic acid). Peptide elution was carried out with a linear gradient of 7–40% B in 45 min (A: 0.1% FA; B: ACN, 0.1% FA) at a flow rate of 300 nl/min. Peptides were analyzed in a mass spectrometer nanoESI qQTOF (6600plus TripleTOF; ABSCIEX) using positive electrospray ionization (ESI) at an ion source temperature of 200°C. The tripleTOF was operated in swath mode in which a 0.050-s TOF MS scan from 350 to 1,250 m/z was performed, followed by 0.080-s product ion scans from 350 to 1,250 m/z. 100 variable windows from 400 to 1,250 m/z were acquired throughout the experiment. The total cycle time was 2.79 s.

The processing settings used for the peptide selection were as follows: detect at least 20 peptides per protein, six or more transitions per peptide, 95% peptide confidence threshold, and 1% false discovery rate threshold; modified peptides were excluded. Only proteins that met these criteria and were detected in all strains were analyzed in this study.

To analyze the proteomic data, protein areas were normalized by the total sum of the areas of all the quantified proteins. To obtain the GO terms overrepresented in the different groups of proteins, the ratio 41°C/25°C was calculated for each replicate and strain. Then each 41°C/25°C ratio of each temperature-sensitive mutant was divided by the ratio 41°C/25°C of wild-type strain so that those with a value >1 are upregulated in temperature-sensitive mutant with respect to wild-type, while those with a value <1 are downregulated. Statistical significance was measured by Student's *t* test; only statistically significant proteins (P value Student's *t* test < 0.05) were analyzed.

nLuc reporter assays

nLuc synthesis assays were performed as detailed in Guzikowski et al. (2022). Briefly, cells were grown at 25°C in YPD media to an exponential OD_{600} 0.4 and then transferred to 37°C for 4 h. Doxycycline was added to a final concentration of 10 µg/ml to induce the expression of the nLuc reporter of the pAG306 series vectors and preincubated for 5 min at room temperature. The nLuc activity was measured using furimazine as the nLuc highly specific substrate. A 90-µl volume of each culture and 10 µl of the furimazine (1 in 200 dilution; Promega) were incubated in a Cellstar non-transparent white 96-well microplate for 1 h and the bioluminescence intensity was monitored with a Tecan Infinite 200 PRO plate reader every 30 s. All the bioluminescence measurements were acquired at 460 nm, the peak emission wavelength of nLuc. Obtained data were linearized using Schleif plots to estimate the minimum reaction time required for complete translation (Schleif et al., 1973). The reaction time of the nLuc reporter alone was subtracted from the reaction time of the corresponding Tim50-nLuc fusion to calculate the time required for translating the different Tim50 sequence versions. At least three biological replicates of each nLuc construct were analyzed.

RT-qPCR analysis

For the analysis of the mRNA levels, total RNAs were isolated from yeast cells following the phenol:chloroform protocol. Briefly, a volume of an exponential phase culture corresponding to 10 OD_{600} units was harvested and flash-frozen. Cells were resuspended in 500 µl of cold LETS buffer (LiCl 0.1 M, EDTA pH 8.0 10 mM, Tris-HCl pH 7.4 10 mM, SDS 0.2%) and transferred into a screw-cap tube already containing 500 µl of sterile glass beads and 500 µl of phenol:chloroform (5:1). Then, cells were broken using the Precellys 24 tissue homogenizer (Bertin Technologies) and centrifugated. The supernatant was transferred into a new tube containing 500 µl of phenol:chloroform (5:1) and then to a tube containing 500 µl of chloroform:isoamyl alcohol (25:1). RNA from the top phase was precipitated and finally dissolved in water for later quantification and quality control with Nanodrop device (Thermo Fisher Scientific).

The reverse transcription and qPCR reactions were performed as detailed in Garre et al. (2013). Briefly, 2.5 µg of the total DNAse-I (Cat# 04536282001; Roche)-treated RNA was retrotranscribed using an oligo $d(T)_{18}$ with Maxima Reverse

Transcriptase (Cat# EP0741; Thermo Fisher Scientific). cDNA was labeled with SYBR Pre-mix Ex Taq (Tli RNase H Plus, Cat# RR420; Takara) and the Cq values were obtained from the CFX96 TouchTM Real-Time PCR Detection System (BioRad). Endogenous *ACT1* mRNA levels were used for normalization. At least three biological replicates of each sample were analyzed and the specific primers designed to amplify gene fragments of interest are listed in Table S4.

Western blotting

For yeast protein content analysis by western blotting, we followed the protocol described in Zuzuarregui et al. (2015). Briefly, a cell culture volume corresponding to 10 OD_{600} units was harvested by centrifugation. For protein extraction, cell pellets were washed and resuspended in 200 µl of NaOH 0.2 M and incubated at room temperature for 5 min for subsequent centrifugation at 12,000 rpm for 1 min. Samples were then resuspended in 100 µl of 2X-SDS protein loading buffer (24 mM Tris-HCl pH 6.8, 10% glycerol, 0.8% SDS, 5.76 mM β-mercaptoethanol, and 0.04% bromophenol blue) and boiled at 95°C for 5 min. Next, lysates were centrifuged at 3,000 rpm for 10 min at 4°C to remove cell debris and insoluble proteins, and the supernatants were transferred into new tubes and stored at −20°C. The total protein content in the extract was quantified by an OD_{280} estimation in a Nanodrop device (Thermo Fisher Scientific) to load equal protein amounts per sample into the SDS-PAGE gel. The acrylamide percentage of the used SDS-PAGE depended on the molecular weight of the protein of interest.

SDS-PAGE and western blotting were performed using standard procedures (BioRad). Blotting membranes were blocked with 5% skimmed milk in TBS-T (150 mM NaCl, 20 mM Tris, 0.1% Tween20, pH 7.6) for 1 h at room temperature and incubated with primary antibodies overnight at 4°C against either HA (Cat# 12013819001; Roche, RRID:AB_390917), GFP (Cat# 11814460001; Roche, RRID:AB_390913), FLAG (Cat# F1804; Sigma-Aldrich, RRID:AB_262044), Por1 (Cat# ab110326; Abcam, RRID:AB_10865182), Hsp60 (Cat #11101; QED_BIOSCIENCE), H4 (Cat# ab7311; Abcam, RRID:AB_305837), or glucose-6-phosphate dehydrogenase (Cat# A9521; Sigma-Aldrich, RRID:AB_258454). Bound antibodies were detected using the appropriate horseradish peroxidase–conjugated secondary antibodies (Cat# W4011; Promega, RRID:AB_430833; Cat# W4021; Promega, RRID:AB_430834). Chemiluminescent signals were detected with an ECL Prime western blotting detection kit (Cat# GERPN2236; GE Healthcare) and digitally analyzed using ImageQuant LAS 4000 software (RRID:SCR_014246). To capture variation across all samples, the signal in each lane was normalized to the mean signal across all lanes in a single blot. Then, the resulting signal of bands was normalized against the corresponding G6pdh resulting signal. At least three biological replicates of each sample were analyzed.

Fluorescence microscopy and analysis

Yeast cells were grown to a post-diauxic phase in SGal medium, centrifugated, washed, and subjected to standard fluorescence and phase contrast microscopy. For mitochondrial protein localization experiments, cells were imaged using an Eclipse Ti-E microscope (Nikon) with an oil-immersion ×63 objective. Imaging was controlled using NIS-Elements software (RRID:SCR_014329). For mitochondrial aggregates, co-localization experiments, and mitochondrial membrane potential measurements, fluorescence images were acquired using an Axio Imager Z1 fluorescence motorized microscope equipped with a Plan Apochratic ×63/1.4 oil-immersion objective and a 100W mercury lamp (Carl Zeiss). Images were recorded with an AxioCam MRm digital camera (Carl Zeiss). The following excitation and emission wavelengths were used: DAPI (excitation 359 nm; emission 457 nm), GFP (excitation 475 nm; emission 509 nm), MitoTracker Red (excitation 578 nm; emission 600 nm), RFP (excitation 555 nm; emission 583 nm), mCherry (excitation 587 nm; emission 610 nm), and Nile Red (excitation 460 nm; emission 582 nm). The same exposure times were used to acquire all images. To analyze mitochondrial membrane potential, cells were incubated with 0.5 µM MitoTracker Red CMXRos (Cat#M46752; Thermo Fisher Scientific) for 30 min, washed, and subjected to the microscope. To analyze Pdr5 activity, cells were incubated with 3.5 µM Nile Red (Cat# N1142; Thermo Fisher Scientific) for 15 min, washed, and subjected to the microscope. To study nuclei localization, cells were incubated with 1 µg/ml DAPI (Cat# 62247; Thermo Fisher Scientific) for 20 min in the dark, washed, and subjected to the microscope.

For single molecule mRNA visualization with mitochondria, cells were imaged by an Eclipse Ti2-E Spinning Disk Confocal with Yokogawa CSU-X1 (Yokogawa) with 50-µm pinholes located at the Nikon Imaging Center University of California San Diego. Imaging was performed using SR HP APO TIRF 100 × 1.49 NA oil objective with the correction collar set manually for each experiment (pixel size 0.074 mm). Z-stacks (300-nm steps) were acquired by a Prime 95B sCMOS camera (Photometrics). Imaging was controlled using NIS-Elements software (RRID:SCR_014329).

All the imaging analysis was performed on ImageJ software (RRID:SCR_003070). To analyze the presence of protein aggregates, cells were manually counted for the presence of 0, 1, 2, or >3 aggregates. For the analysis of fluorescence intensity, signal regions of interest were manually outlined around cells using the "Freehand" selection tool in ImageJ (RRID:SCR_003070) on differential interference contrast (DIC) images. After background substraction, the amount of Pdr5-GFP, Tim50-GFP, Tim50ΔPro-GFP, Mitotracker, and Red Nile (total fluorescence intensity) was quantified in the whole cell. At least 150 single cells were scored from three independent experiments.

Polyribosome profile analysis

For polysome fractioning, cells were grown at 25°C to post-diauxic phase in SGal medium and transferred to 37°C for 4 h for the experiments requiring temperature-sensitive strains. Cell extractions and polysome gradients were performed as described by Garre et al. (2012), Ramos-Alonso et al. (2018). Briefly, a culture volume corresponding to an OD_{600} of 100 was chilled for 5 min on ice in the presence of 0.1 mg/ml CHX. Cells were centrifuged at 4,400 rpm for 3 min at 4°C and washed twice with 2 ml of lysis buffer (20 mM Tris-HCl pH 8, 140 mM KCl, 5 mM $MgCl_2$, 0.5 mM DTT, 1% Triton X-100, 0.1 mg/ml CHX, and 0.5 mg/ml heparin). Cells were resuspended in 700 µl of lysis buffer and added to a tube already containing 500 µl of

glass beads. Cells were mechanically disrupted by vortexing eight times for 30 s with 30 s of incubation on ice in between. Then, lysates were cleared by centrifugation at 5,000 rpm for 5 min at 4°C, and the supernatant was recovered. After centrifugation at 8,000 rpm for 5 min at 4°C, the RNA was recovered and its concentration was estimated using a Nanodrop device (Thermo Fisher Scientific). Glycerol was added to all the samples to a final concentration of 5% and extracts were flash-frozen and stored at −80°C. Samples of 10 $A_{260\ nm}$ units were loaded onto 5–50% sucrose gradients and separated by ultracentrifugation for 2 h 40 min at 35,000 rpm in a Beckman SW41Ti rotor at 4°C. Then, gradients were fractionated by isotonic pumping of 60% sucrose from the bottom, and twenty-two 0.5 ml samples were recovered. The polysome profiles were monitored by UV detection at 260 nm using a density gradient fractionation system (Teledyne Isco). RNAs were extracted using SpeedTools Total RNA Extraction kit (Cat# 21.212-4210; Biotools B&M Labs) with the rDNAse treatment after the RNA elution step. Specific mRNAs were analyzed by RT-qPCR using specific primers (listed in Table S4) and represented as a percentage of total. A calibrating efficiency standard curve was obtained for each set of primers after the initial setup, so slight differences in amplification efficiencies were taken into account. No spike in controls was used to normalize since no significant differences were found when using or not these controls. Three biological replicates were performed for each polyribosome profile and a representative profile is shown.

For graphical representations, mRNAs were classified as short (<600 bp) or long (>600 bp) ORF length (Table S5) on the basis of specific mRNA profiles obtained by qPCR analysis. mRNAs with short lengths behaved similarly and 2n-3n fractions were selected as light fractions since the main polysomal peak under normal conditions appeared among 4n-5n fractions. In this line, long-length mRNAs also behaved similarly between them, and 2n to 8n fractions were selected as light fractions since the main polysomal peak under normal conditions appeared right after the 8n fraction. The three fractions previous to the 2n-3n/2n-8n ones were selected as monosomal fractions for qPCR analysis.

Proteomic data accession

The mass spectrometry proteomics data have been deposited to the ProteomeXchange Consortium (Deutsch et al., 2023) via the Pride-asap (RRID:SCR_012052) (Perez-Riverol et al., 2022) partner repository with the dataset identifier PXD043905.

Online supplemental material

Fig. S1 shows proteomic analysis upon eIF5A depletion and shows the downregulation of yeast mitochondrial proteins. Fig. S2 shows that temperature-sensitive eIF5A mutants do not show defects in the translation of mitochondrial proteins at permissive temperatures. Fig. S3 shows that PDR5 activation in eIF5A mutant results in the cellular extrusion of Nile Red fluorescent dye. Fig. S4 shows that ribosome stalling at *TIM50* mRNA upon eIF5A depletion does not change mRNA levels nor its mitochondrial localization. Fig. S5 shows that protein half-life and mRNA levels of Tim50 and Tim50ΔPro are not affected by eIF5A depletion. Table S1 shows mitochondrial proteins detected in the proteomic analysis with a statistical significant different expression between eIF5A mutant and wild-type. Table S2 shows the yeast strains used in this study. Table S3 shows the plasmids used in this study. Table S4 shows the oligonucleotides used in this study. Table S5 shows the main characteristics of mRNAs analyzed by polysome profiling. Table S6 shows co-translationally inserted mitoproteins with the largest shift of ribosome distribution upon eIF5A depletion.

Acknowledgments

The proteomic analysis was performed in the proteomics facility of SCSIE University of Valencia. We thank Oreto Antúnez and M. Luz Valero from this Proteomics Service.

Work was supported by grants PID2020-120066RB-I00 and PID2023-152214NB-I00 funded by the Ministry of Science, Innovation and Universities (MCIN)/Agencia Estatal de Investigación (AEI) to P. Alepuz. This work was supported, in part, by the National Institutes of Health R35GM128798 to B.M. Zid. This research was also funded by Generalitat Valenciana (AICO/2020/086 and CIAICO/2022/237) to P. Alepuz. M. Barba-Aliaga is a recipient of a predoctoral fellowship (FPU2017/03542) funded by MCIN/AEI/10.13039/501100011033 and by the European Social Fund. Authors acknowledge support by all members of Gene Expression: DNAtoProtein lab.

Author contributions: M. Barba-Aliaga: Conceptualization, Investigation, Methodology, Project administration, Resources, Supervision, Validation, Visualization, Writing - original draft, Writing - review & editing, V. Bernal: Formal analysis, Investigation, Visualization, C. Rong: Investigation, Methodology, M.E. Volfbeyn: Investigation, Validation, K. Zhang: Investigation, B.M. Zid: Conceptualization, Formal analysis, Funding acquisition, Investigation, Project administration, Supervision, Writing - original draft, Writing - review & editing, P. Alepuz: Conceptualization, Formal analysis, Funding acquisition, Project administration, Resources, Supervision, Writing - original draft, Writing - review & editing.

Disclosures: The authors declare no competing interests exist.

Submitted: 18 April 2024
Revised: 29 July 2024
Accepted: 19 September 2024

References

Aviner, R., T.-T. Lee, V.B. Masto, K.H. Li, R. Andino, and J. Frydman. 2024. Polyglutamine-mediated ribotoxicity disrupts proteostasis and stress responses in Huntington's disease. *Nat. Cell Biol.* 26:892–902. https://doi.org/10.1038/s41556-024-01414-x

Balaban, R.S., S. Nemoto, and T. Finkel. 2005. Mitochondria, oxidants, and aging. *Cell.* 120:483–495. https://doi.org/10.1016/j.cell.2005.02.001

Barba-Aliaga, M., and P. Alepuz. 2022a. The activator/repressor Hap1 binds to the yeast eIF5A-encoding gene TIF51A to adapt its expression to the mitochondrial functional status. *FEBS Lett.* 596:1809–1826. https://doi.org/10.1002/1873-3468.14366

Barba-Aliaga, M., and P. Alepuz. 2022b. Role of eIF5A in mitochondrial function. *Int. J. Mol. Sci.* 23:1284. https://doi.org/10.3390/ijms23031284

Barba-Aliaga, M., C. Villarroel-Vicente, A. Stanciu, A. Corman, M.T. Martínez-Pastor, and P. Alepuz. 2020. Yeast translation elongation

factor eif5a expression is regulated by nutrient availability through different signalling pathways. *Int. J. Mol. Sci.* 22:219. https://doi.org/10.3390/ijms22010219

Berglund, L.L., X. Hao, B. Liu, J. Grantham, and T. Nyström. 2017. Differential effects of soluble and aggregating polyQ proteins on cytotoxicity and type-1 myosin-dependent endocytosis in yeast. *Sci. Rep.* 7:11328. https://doi.org/10.1038/s41598-017-11102-6

Boengler, K., M. Kosiol, M. Mayr, R. Schulz, and S. Rohrbach. 2017. Mitochondria and ageing: Role in heart, skeletal muscle and adipose tissue. *J. Cachexia Sarcopenia Muscle.* 8:349–369. https://doi.org/10.1002/jcsm.12178

Boos, F., L. Krämer, C. Groh, F. Jung, P. Haberkant, F. Stein, F. Wollweber, A. Gackstatter, E. Zöller, M. van der Laan, et al. 2019. Mitochondrial protein-induced stress triggers a global adaptive transcriptional programme. *Nat. Cell Biol.* 21:442–451. https://doi.org/10.1038/s41556-019-0294-5

Borst, P., and L.A. Grivell. 1973. Mitochondrial nucleic acids. *Biochimie*. 55:801–804. https://doi.org/10.1016/S0300-9084(73)80032-X

Bykov, Y.S., D. Rapaport, J.M. Herrmann, and M. Schuldiner. 2020. Cytosolic events in the biogenesis of mitochondrial proteins. *Trends Biochem. Sci.* 45:650–667. https://doi.org/10.1016/j.tibs.2020.04.001

Cenini, G., C. Rüb, M. Bruderek, and W. Voos. 2016. Amyloid β-peptides interfere with mitochondrial preprotein import competence by a coaggregation process. *Mol. Biol. Cell*. 27:3257–3272. https://doi.org/10.1091/mbc.E16-05-0313

Chaudhuri, M., A. Tripathi, and F.S. Gonzalez. 2021. Diverse functions of tim50, a component of the mitochondrial inner membrane protein translocase. *Int. J. Mol. Sci.* 22:7779. https://doi.org/10.3390/ijms22157779

Christiano, R., N. Nagaraj, F. Fröhlich, and T.C. Walther. 2014. Global proteome turnover analyses of the Yeasts S. cerevisiae and S. pombe. *Cell Rep.* 9:1959–1965. https://doi.org/10.1016/j.celrep.2014.10.065

Deutsch, E.W., N. Bandeira, Y. Perez-Riverol, V. Sharma, J.J. Carver, L. Mendoza, D.J. Kundu, S. Wang, C. Bandla, S. Kamatchinathan, et al. 2023. The ProteomeXchange consortium at 10 years: 2023 update. *Nucleic Acids Res.* 51:D1539–D1548. https://doi.org/10.1093/nar/gkac1040

Fukasawa, Y., J. Tsuji, S.-C. Fu, K. Tomii, P. Horton, and I. Kenichiro. 2015. MitoFates: Improved prediction of mitochondrial targeting sequences and their cleavage sites. *Mol. Cell. Proteomics*. 14:1113–1126. https://doi.org/10.1074/mcp.M114.043083

Garre, E., L. Romero-Santacreu, M. Barneo-Muñoz, A. Miguel, J.E. Pérez-Ortín, and P. Alepuz. 2013. Nonsense-mediated mRNA decay controls the changes in yeast ribosomal protein pre-mRNAs levels upon osmotic stress. *PLoS One.* 8:e61240. https://doi.org/10.1371/journal.pone.0061240

Garre, E., L. Romero-Santacreu, N. De Clercq, N. Blasco-Angulo, P. Sunnerhagen, and P. Alepuz. 2012. Yeast mRNA cap-binding protein Cbc1/Sto1 is necessary for the rapid reprogramming of translation after hyperosmotic shock. *Mol. Biol. Cell*. 23:137–150. https://doi.org/10.1091/mbc.e11-05-0419

Gates, S.N., A.L. Yokom, J.B. Lin, M.E. Jackrel, A.N. Rizo, N.M. Kendsersky, C.E. Buell, E.A. Sweeny, K.L. Mack, E. Chuang, et al. 2017. Ratchet-like polypeptide translocation mechanism of the AAA+ disaggregase Hsp104. *Science*. 357:273–279. https://doi.org/10.1126/science.aan1052

Gietz, D., A. St Jean, R.A. Woods, and R.H. Schiestl. 1992. Improved method for high efficiency transformation of intact yeast cells. *Nucleic Acids Res.* 20:1425. https://doi.org/10.1093/nar/20.6.1425

Giraud, S., T. Kerforne, J. Zely, V. Ameteau, P. Couturier, M. Tauc, and T. Hauet. 2020. The inhibition of eIF5A hypusination by GC7, a preconditioning protocol to prevent brain death-induced renal injuries in a preclinical porcine kidney transplantation model. *Am. J. Transpl.* 20:3326–3340. https://doi.org/10.1111/ajt.15994

Gutierrez, E., B.S. Shin, C.J. Woolstenhulme, J.R. Kim, P. Saini, A.R. Buskirk, and T.E. Dever. 2013. eIF5A promotes translation of polyproline motifs. *Mol. Cell*. 51:35–45. https://doi.org/10.1016/j.molcel.2013.04.021

Guzikowski, A.R., A.T. Harvey, J. Zhang, S. Zhu, K. Begovich, M.H. Cohn, J.E. Wilhelm, and B.M. Zid. 2022. Differential translation elongation directs protein synthesis in response to acute glucose deprivation in yeast. *RNA Biol.* 19:636–649. https://doi.org/10.1080/15476286.2022.2065784

Haastrup, M.O., K.S. Vikramdeo, S. Singh, A.P. Singh, and S. Dasgupta. 2023. The journey of mitochondrial protein import and the roadmap to follow. *Int. J. Mol. Sci.* 24:2479. https://doi.org/10.3390/ijms24032479

Hansen, K.G., and J.M. Herrmann. 2019. Transport of proteins into mitochondria. *Protein J.* 38:330–342. https://doi.org/10.1007/s10930-019-09819-6

Hill, S.M., S. Hanzén, and T. Nyström. 2017. Restricted access: Spatial sequestration of damaged proteins during stress and aging. *EMBO Rep.* 18:377–391. https://doi.org/10.15252/embr.201643458

Hou, W., V. Harjono, A.T. Harvey, A.R. Subramaniam, and B.M. Zid. 2023. Quantification of elongation stalls and impact on gene expression in yeast. *RNA*. 29:1928–1938. https://doi.org/10.1261/rna.079663.123

Jenkins, Z.A., P.G. Hååg, and H.E. Johansson. 2001. Human eIF5A2 on chromosome 3q25-q27 is a phylogenetically conserved vertebrate variant of eukaryotic translation initiation factor 5A with tissue-specific expression. *Genomics*. 71:101–109. https://doi.org/10.1006/geno.2000.6418

Kellems, R.E., and R.A. Butow. 1972. Cytoplasmic-type 80 S ribosomes associated with yeast mitochondria. I. Evidence for ribosome binding sites on yeast mitochondria. *J. Biol. Chem.* 247:8043–8050. https://doi.org/10.1016/S0021-9258(20)81806-7

Krämer, L., N. Dalheimer, M. Räschle, Z. Storchová, J. Pielage, F. Boos, and J.M. Herrmann. 2023. MitoStores: Chaperone-controlled protein granules store mitochondrial precursors in the cytosol. *EMBO J.* 42:e112309. https://doi.org/10.15252/embj.2022112309

Lenkiewicz, A.M., M. Krakowczyk, and P. Bragoszewski. 2021. Cytosolic quality control of mitochondrial protein precursors-the early stages of the organelle biogenesis. *Int. J. Mol. Sci.* 23:7. https://doi.org/10.3390/ijms23010007

Li, J., and B. Sha. 2015. The structure of Tim50(164-361) suggests the mechanism by which Tim50 receives mitochondrial presequences. *Acta Crystallogr. F Struct. Biol. Commun.* 71:1146–1151. https://doi.org/10.1107/S2053230X15013102

Li, T., B. Belda-Palazón, A. Ferrando, and P. Alepuz. 2014. Fertility and polarized cell growth depends on eIF5A for translation of polyproline-rich formins in Saccharomyces cerevisiae. *Genetics*. 197:1191–1200. https://doi.org/10.1534/genetics.114.166926

Li, Z., F.J. Vizeacoumar, S. Bahr, J. Li, J. Warringer, F.S. Vizeacoumar, R. Min, B. Vandersluis, J. Bellay, M. Devit, et al. 2011. Systematic exploration of essential yeast gene function with temperature-sensitive mutants. *Nat. Biotechnol.* 29:361–367. https://doi.org/10.1038/nbt.1832

Liu, J., X. Zhan, M. Li, G. Li, P. Zhang, Z. Xiao, M. Shao, F. Peng, R. Hu, and Z. Chen. 2012. Mitochondrial proteomics of nasopharyngeal carcinoma metastasis. *BMC Med. Genomics*. 5:62. https://doi.org/10.1186/1755-8794-5-62

Longtine, M.S., A. McKenzie III, D.J. Demarini, N.G. Shah, A. Wach, A. Brachat, P. Philippsen, and J.R. Pringle. 1998. Additional modules for versatile and economical PCR-based gene deletion and modification in Saccharomyces cerevisiae. *Yeast*. 14:953–961. https://doi.org/10.1002/(SICI)1097-0061(199807)14:10<953:AID-YEA293>3.0.CO;2-U

Mårtensson, C.U., C. Priesnitz, J. Song, L. Ellenrieder, K.N. Doan, F. Boos, A. Floerchinger, N. Zufall, S. Oeljeklaus, B. Warscheid, and T. Becker. 2019. Mitochondrial protein translocation-associated degradation. *Nature*. 569:679–683. https://doi.org/10.1038/s41586-019-1227-y

Masser, A.E., G. Kandasamy, J.M. Kaimal, and C. Andréasson. 2016. Luciferase NanoLuc as a reporter for gene expression and protein levels in Saccharomyces cerevisiae. *Yeast*. 33:191–200. https://doi.org/10.1002/yea.3155

Melis, N., I. Rubera, M. Cougnon, S. Giraud, B. Mograbi, A. Belaid, D.F. Pisani, S.M. Huber, S. Lacas-Gervais, K. Fragaki, et al. 2017. Targeting eIF5A hypusination prevents anoxic cell death through mitochondrial silencing and improves kidney transplant outcome. *J. Am. Soc. Nephrol.* 28:811–822. https://doi.org/10.1681/ASN.2016010012

Miyake, T., S. Pradeep, S.Y. Wu, R. Rupaimoole, B. Zand, Y. Wen, K.M. Gharpure, A.S. Nagaraja, W. Hu, M.S. Cho, et al. 2015. XPO1/CRM1 inhibition causes antitumor effects by mitochondrial accumulation of eIF5A. *Clin. Cancer Res.* 21:3286–3297. https://doi.org/10.1158/1078-0432.CCR-14-1953

Mokranjac, D., and W. Neupert. 2009. Thirty years of protein translocation into mitochondria: Unexpectedly complex and still puzzling. *Biochim. Biophys. Acta*. 1793:33–41. https://doi.org/10.1016/j.bbamcr.2008.06.021

Nowicka, U., P. Chroscicki, K. Stroobants, M. Sladowska, M. Turek, B. Uszczynska-Ratajczak, R. Kundra, T. Goral, M. Perni, C.M. Dobson, et al. 2021. Cytosolic aggregation of mitochondrial proteins disrupts cellular homeostasis by stimulating the aggregation of other proteins. *Elife*. 10:e65484. https://doi.org/10.7554/eLife.65484

Park, M.H., R.K. Kar, S. Banka, A. Ziegler, and W.K. Chung. 2021. Post-translational formation of hypusine in eIF5A: Implications in human neurodevelopment. *Amino Acids*. 54:485–499. https://doi.org/10.1007/s00726-021-03023-6

Pelechano, V., and P. Alepuz. 2017. eIF5A facilitates translation termination globally and promotes the elongation of many non polyproline-specific tripeptide sequences. *Nucleic Acids Res.* 45:7326–7338. https://doi.org/10.1093/nar/gkx479

Pereira, K.D., L. Tamborlin, L. Meneguello, A.R.G. de Proença, I.C. Almeida, R.F. Lourenço, and A.D. Luchessi. 2016. Alternative start codon connects

eIF5A to mitochondria. *J. Cell. Physiol.* 231:2682–2689. https://doi.org/10.1002/jcp.25370

Perez-Riverol, Y., J. Bai, C. Bandla, D. García-Seisdedos, S. Hewapathirana, S. Kamatchinathan, D.J. Kundu, A. Prakash, A. Frericks-Zipper, M. Eisenacher, et al. 2022. The PRIDE database resources in 2022: A hub for mass spectrometry-based proteomics evidences. *Nucleic Acids Res.* 50: D543–D552. https://doi.org/10.1093/nar/gkab1038

Puleston, D.J., M.D. Buck, R.I. Klein Geltink, R.L. Kyle, G. Caputa, D. O'Sullivan, A.M. Cameron, A. Castoldi, Y. Musa, A.M. Kabat, et al. 2019. Polyamines and eIF5A hypusination modulate mitochondrial respiration and macrophage activation. *Cell Metab.* 30:352–363.e8. https://doi.org/10.1016/j.cmet.2019.05.003

Ramos-Alonso, L., A.M. Romero, M.À. Soler, A. Perea-García, P. Alepuz, S. Puig, and M.T. Martínez-Pastor. 2018. Yeast Cth2 protein represses the translation of ARE-containing mRNAs in response to iron deficiency. *PLoS Genet.* 14:e1007476. https://doi.org/10.1371/journal.pgen.1007476

Roger, A.J., S.A. Muñoz-Gómez, and R. Kamikawa. 2017. The origin and diversification of mitochondria. *Curr. Biol.* 27:R1177–R1192. https://doi.org/10.1016/j.cub.2017.09.015

Sanchez, Y., and S.L. Lindquist. 1990. HSP104 required for induced thermotolerance. *Science.* 248:1112–1115. https://doi.org/10.1126/science.2188365

Sarkadi, B., L. Homolya, G. Szakács, and A. Váradi. 2006. Human multidrug resistance ABCB and ABCG transporters: Participation in a chemoimmunity defense system. *Physiol. Rev.* 86:1179–1236. https://doi.org/10.1152/physrev.00037.2005

Schäfer, J.A., S. Bozkurt, J.B. Michaelis, K. Klann, and C. Münch. 2022. Global mitochondrial protein import proteomics reveal distinct regulation by translation and translocation machinery. *Mol. Cell.* 82:435–446.e7. https://doi.org/10.1016/j.molcel.2021.11.004

Schleif, R., W. Hess, S. Finkelstein, and D. Ellis. 1973. Induction kinetics of the L-arabinose operon of Escherichia coli. *J. Bacteriol.* 115:9–14. https://doi.org/10.1128/jb.115.1.9-14.1973

Schmidt, O., N. Pfanner, and C. Meisinger. 2010. Mitochondrial protein import: From proteomics to functional mechanisms. *Nat. Rev. Mol. Cell Biol.* 11:655–667. https://doi.org/10.1038/nrm2959

Schnier, J., H.G. Schwelberger, Z. Smit-McBride, H.A. Kang, and J.W. Hershey. 1991. Translation initiation factor 5A and its hypusine modification are essential for cell viability in the yeast Saccharomyces cerevisiae. *Mol. Cell. Biol.* 11:3105–3114. https://doi.org/10.1128/mcb.11.6.3105

Schuller, A.P., C.C.C. Wu, T.E. Dever, A.R. Buskirk, and R. Green. 2017. eIF5A functions globally in translation elongation and termination. *Mol. Cell.* 66:194–205.e5. https://doi.org/10.1016/j.molcel.2017.03.003

Shakya, V.P.S., W.A. Barbeau, T. Xiao, C.S. Knutson, M.H. Schuler, and A.L. Hughes. 2021. A nuclear-based quality control pathway for non-imported mitochondrial proteins. *Elife.* 10:e61230. https://doi.org/10.7554/eLife.61230

Topf, U., I. Suppanz, L. Samluk, L. Wrobel, A. Böser, P. Sakowska, B. Knapp, M.K. Pietrzyk, A. Chacinska, and B. Warscheid. 2018. Quantitative proteomics identifies redox switches for global translation modulation by mitochondrially produced reactive oxygen species. *Nat. Commun.* 9: 324. https://doi.org/10.1038/s41467-017-02694-8

Tsuboi, T., M.P. Viana, F. Xu, J. Yu, R. Chanchani, X.G. Arceo, E. Tutucci, J. Choi, Y.S. Chen, R.H. Singer, et al. 2020. Mitochondrial volume fraction and translation duration impact mitochondrial mRNA localization and protein synthesis. *Elife.* 9:e57814. https://doi.org/10.7554/eLife.57814

Vögtle, F.N., S. Wortelkamp, R.P. Zahedi, D. Becker, C. Leidhold, K. Gevaert, J. Kellermann, W. Voos, A. Sickmann, N. Pfanner, and C. Meisinger. 2009. Global analysis of the mitochondrial N-proteome identifies a processing peptidase critical for protein stability. *Cell.* 139:428–439. https://doi.org/10.1016/j.cell.2009.07.045

Wang, X., and X.J. Chen. 2015. A cytosolic network suppressing mitochondria-mediated proteostatic stress and cell death. *Nature.* 524:481–484. https://doi.org/10.1038/nature14859

Weidberg, H., and A. Amon. 2018. MitoCPR—A surveillance pathway that protects mitochondria in response to protein import stress. *Science.* 360: eaan4146. https://doi.org/10.1126/science.aan4146

Wiedemann, N., and N. Pfanner. 2017. Mitochondrial machineries for protein import and assembly. *Annu. Rev. Biochem.* 86:685–714. https://doi.org/10.1146/annurev-biochem-060815-014352

Williams, C.C., C.H. Jan, and J.S. Weissman. 2014. Targeting and plasticity of mitochondrial proteins revealed by proximity-specific ribosome profiling. *Science.* 346:748–751. https://doi.org/10.1126/science.1257522

Wrobel, L., U. Topf, P. Bragoszewski, S. Wiese, M.E. Sztolsztener, S. Oeljeklaus, A. Varabyova, M. Lirski, P. Chroscicki, S. Mroczek, et al. 2015. Mistargeted mitochondrial proteins activate a proteostatic response in the cytosol. *Nature.* 524:485–488. https://doi.org/10.1038/nature14951

Zhang, L., and A. Hach. 1999. Molecular mechanism of heme signaling in yeast: The transcriptional activator Hap1 serves as the key mediator. *Cell. Mol. Life Sci.* 56:415–426. https://doi.org/10.1007/s000180050442

Zhang, Y., D. Su, J. Zhu, M. Wang, Y. Zhang, Q. Fu, S. Zhang, and H. Lin. 2022. Oxygen level regulates N-terminal translation elongation of selected proteins through deoxyhypusine hydroxylation. *Cell Rep.* 39:110855. https://doi.org/10.1016/j.celrep.2022.110855

Zhu, M., X. Dai, and Y.P. Wang. 2016. Real time determination of bacterial in vivo ribosome translation elongation speed based on LacZα complementation system. *Nucleic Acids Res.* 44:e155. https://doi.org/10.1093/nar/gkw698

Zuzuarregui, A., T. Li, C. Friedmann, G. Ammerer, and P. Alepuz. 2015. Msb2 is a Ste11 membrane concentrator required for full activation of the HOG pathway. *Biochim. Biophys. Acta.* 1849:722–730. https://doi.org/10.1016/j.bbagrm.2015.02.001

JCB

Supplemental material

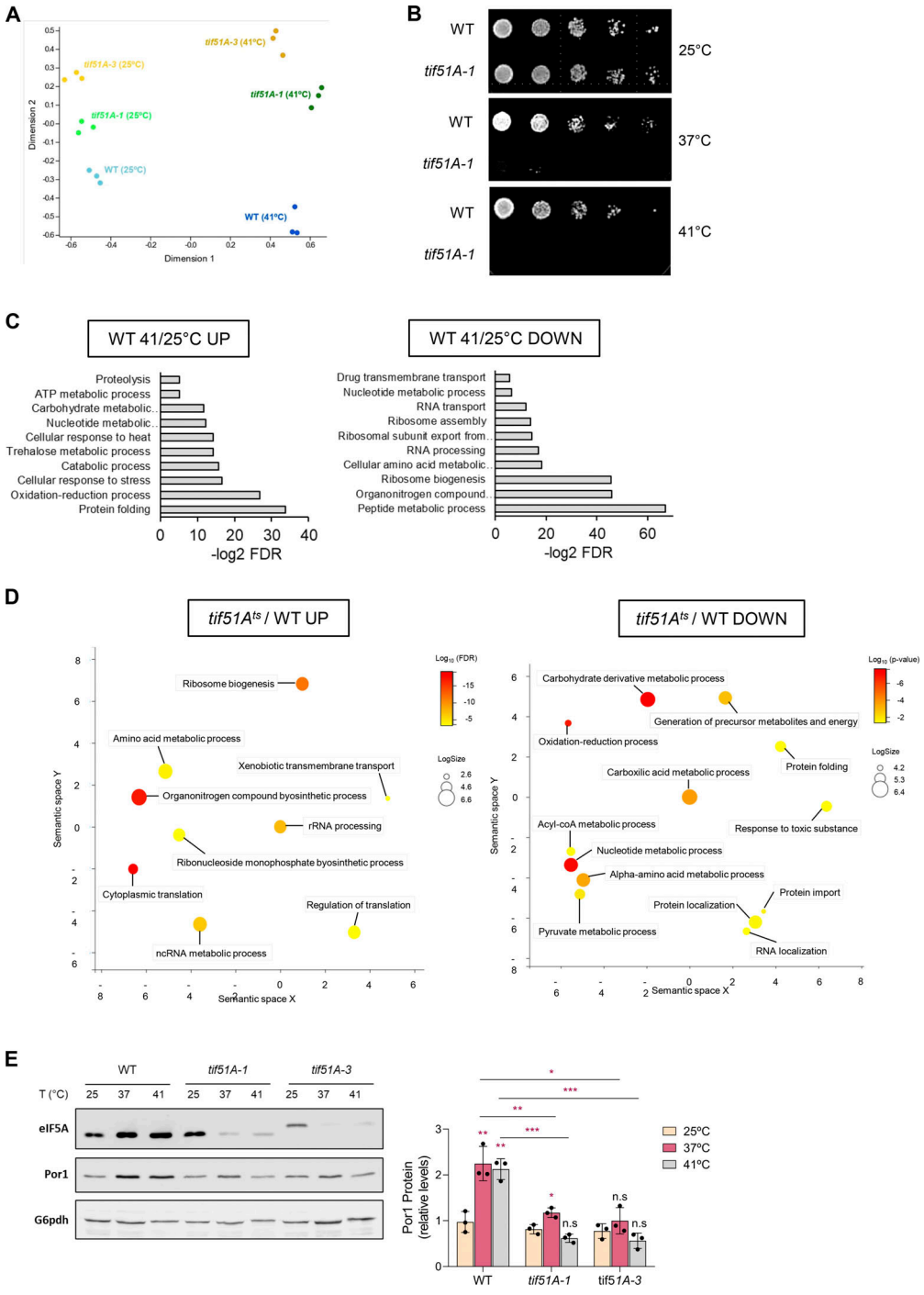

Figure S1. **Proteomic analysis upon eIF5A depletion. (A)** MDS-plot showing all replicates for each strain and condition studied in the proteomic analysis. **(B)** Growth of the wild-type and *tif51A-1* strains was tested in YPD media at the indicated temperatures. **(C)** Biological process overrepresented in proteins up- or downregulated significantly in wild-type cells at 41°C. GO Term analysis was done using the STRING tool, and a total of 272 proteins up- (left) and 154 proteins downregulated (right) significantly in WT 41°C compared with WT 25°C were analyzed. **(D)** Biological process GO terms overrepresented in relative up- (left) or downregulated (right) proteins in *tif51A*^{ts} versus WT. *tif51A*^{ts} stands for the average values obtained for the two eIF5A temperature-sensitive strains (*tif51A-1* and *tif51A-3*). GO term analysis was done using the STRING tool, in which a total of 292 proteins down- and 135 proteins upregulated significantly in at least one *tif51A*^{ts} with respect to wild-type were analyzed. The web-based tool REVIGO was used to summarize the GO terms. Bubble color indicates the P value of the GO term in the input data set; bubble size indicates the frequency of the GO term in the underlying GO database. **(E)** Wild-type, *tif51A-1*, and *tif51A-3* strains were cultured in YPD at 25°C until early exponential phase and transferred to 25°C, 37°C, or 41°C for 4 h. eIF5A and Por1 protein levels were determined by western blotting (left) and quantified (right). G6pdh levels were used as loading control. A representative image is shown from three independent experiments. Data information: In E, results are presented as mean ± SD from three independent experiments. The statistical significance was measured by using a two-tailed Student's *t* test. *P < 0.05, **P < 0.001, ***P < 0.001. The asterisks located above the columns of the graph represent a comparison relative to 25°C conditions within the same strain. The asterisks found at the top of the bars additionally indicate comparisons between the indicated strains at the same treatment condition. n.s means no significant differences. Source data are available for this figure: SourceData FS1.

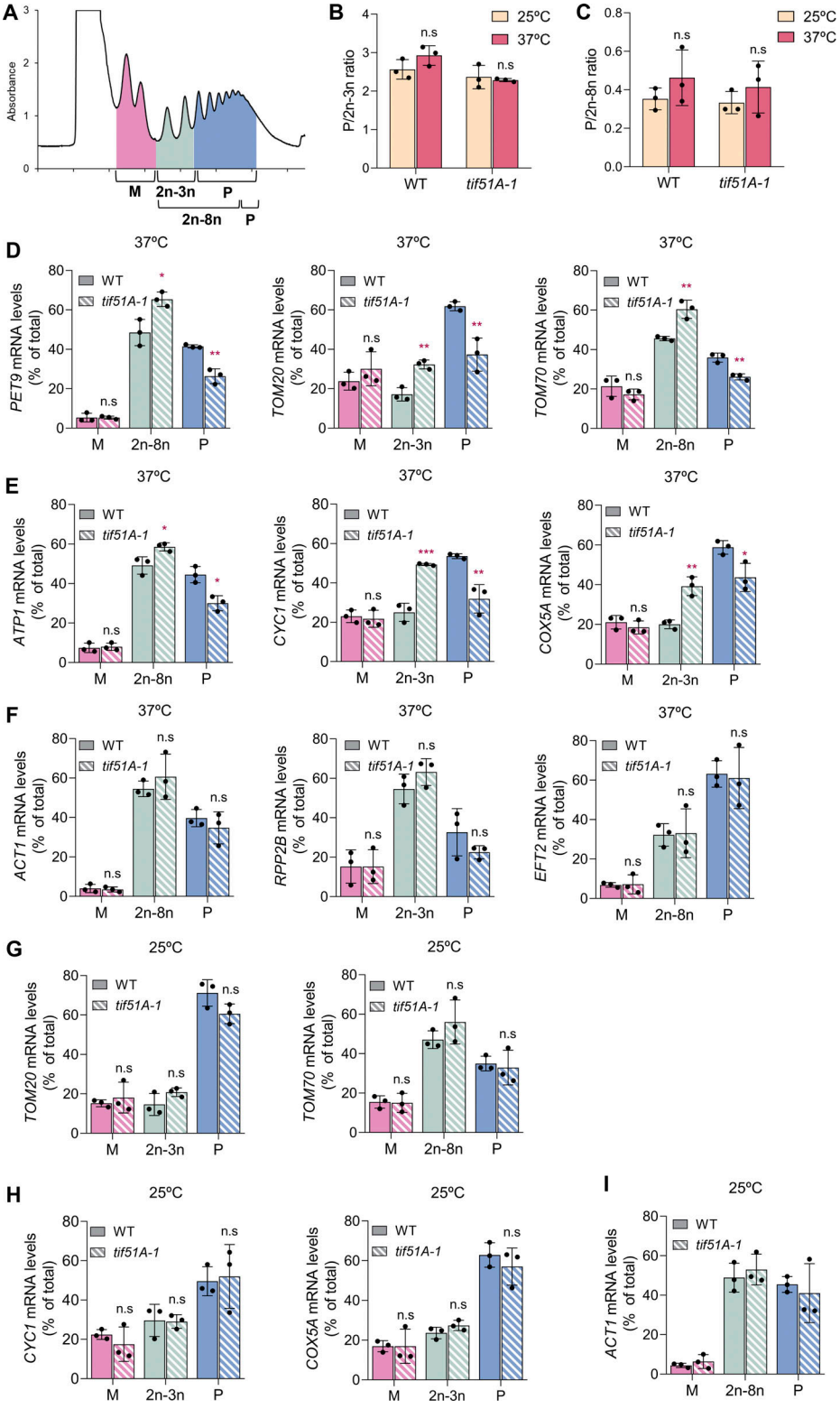

Figure S2. **Translation of mitochondrial proteins is not affected in the *tif51A-1* strain at permissive temperature. (A)** Scheme with the employed area divisions for calculations. **(B)** The average polysomes/2n-3n ratio (P/2n-3n) is represented for each strain at both temperatures. **(C)** The average polysomes/2n-8n ratio (P/2n-8n) is represented for each strain at both temperatures. **(D–F)** The RNA from individual fractions of the polysomes profiles was extracted and the mRNA levels of *PET9*, *TOM20*, *TOM70* (D), *ATP1*, *CYC1*, *COX5A* (E), *ACT1*, *RPP2B*, and *EFT2* (F) were analyzed by RT-qPCR in the corresponding sections at restrictive temperature. **(G–I)** The RNA from individual fractions of the polyribosome profiles was extracted and the mRNA levels of *TOM20*, *TOM70* (G), *CYC1*, COX5A (H), and *ACT1* (I) were analyzed by RT-qPCR in the corresponding sections at permissive temperature. Data information: In B–I, results are presented as mean ± SD from three independent experiments. The statistical significance was measured by using a two-tailed paired Student's *t* test relative to wild-type strain. *P < 0.05, **P < 0.001, ***P < 0.001. n.s means no significant differences.

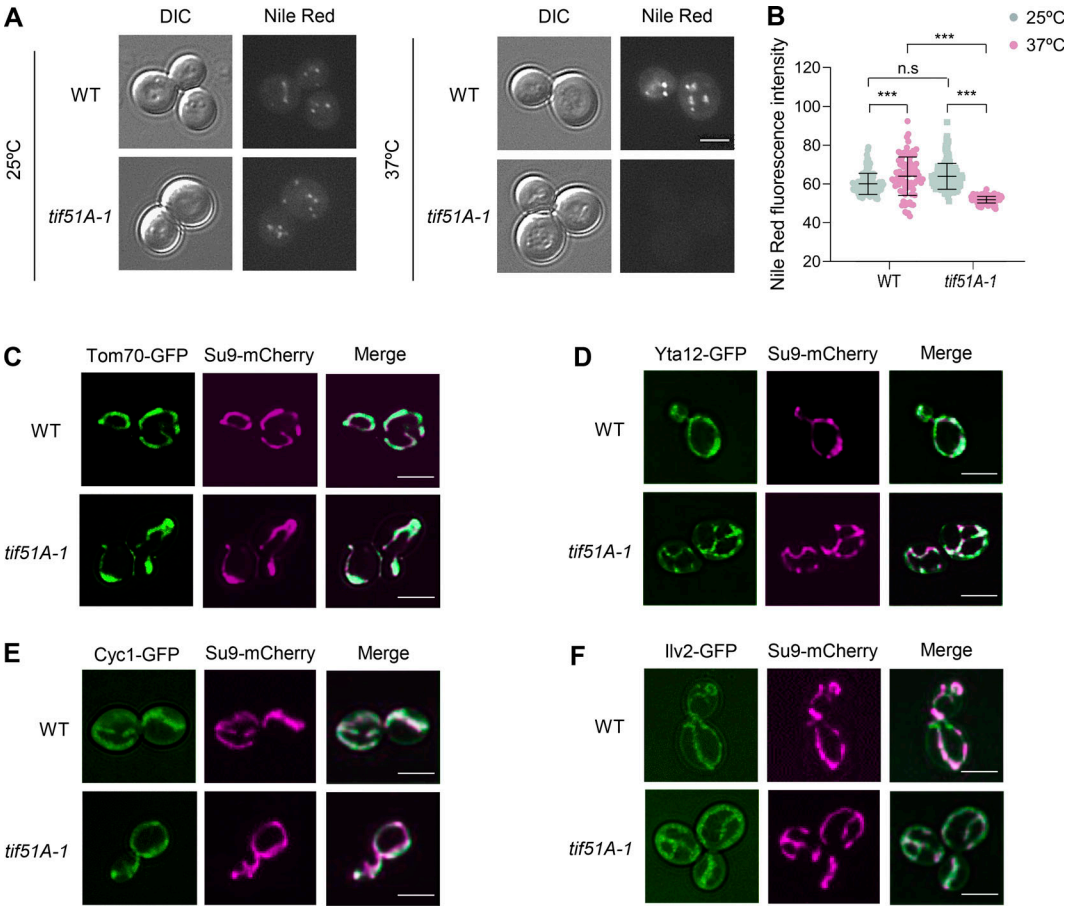

Figure S3. **Nile Red is excluded from the *tif51A-1* mutant because of high Pdr5 pumping activity. (A)** Wild-type strain and *tif51A-1* were cultured in SGal medium at 25°C until reaching post-diauxic phase and then transferred to 25°C or 37°C for 4 h. Then, cells were incubated with Nile Red substrate for 15 min prior to microscopy. A representative image is shown from three independent experiments. Scale bar, 4 µm. **(B)** Quantification of Nile Red fluorescent signal from at least 150 cells. **(C–F)** Wild-type strain and *tif51A-1* expressing Tom70-GFP (C), Yta12-GFP (D), Cyc1-GFP (E), or Ilv2-GFP (F), and Su9-mCherry were cultured in SGal medium at 25°C until reaching post-diauxic phase and subjected to fluorescence microscopy. A representative image is shown from three independent experiments. Scale bar, 4 µm. Data information: In B, results are presented as mean ± SD from three independent experiments. The statistical significance was measured by using a two-tailed paired Student's *t* test. ***P < 0.001. n.s means no significant differences.

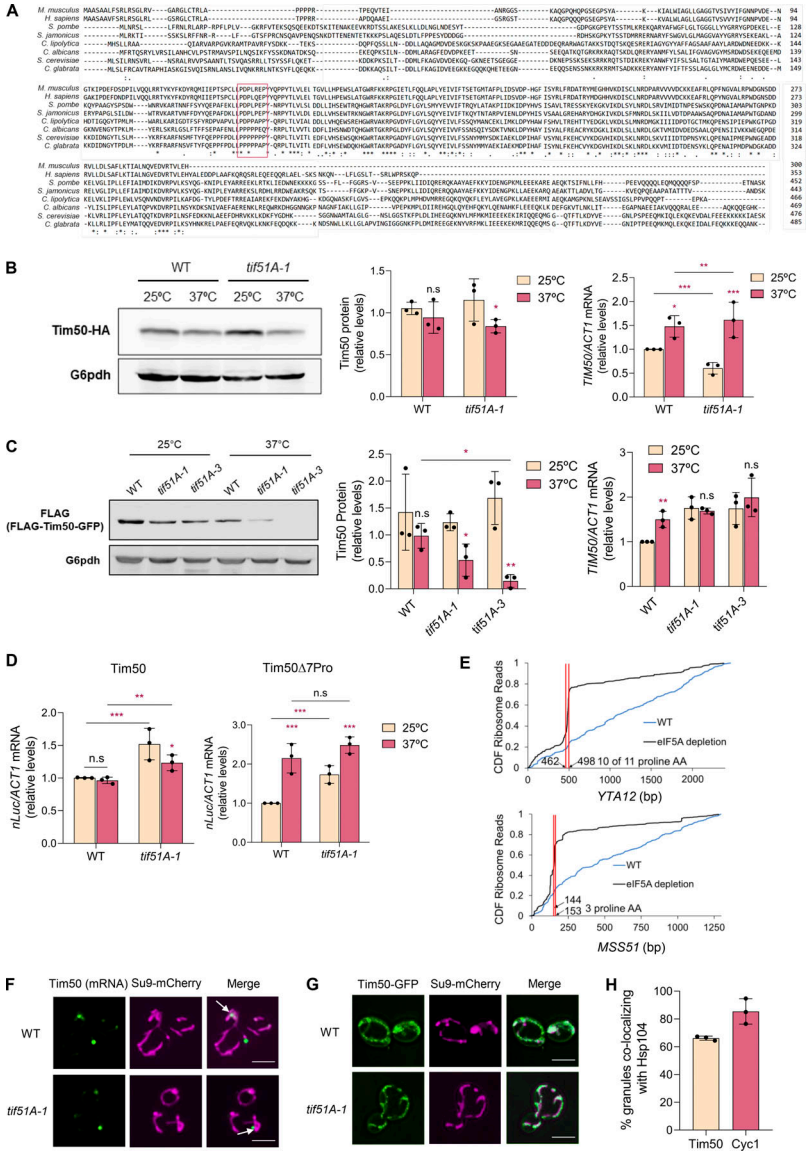

Figure S4. **eIF5A deficiency provokes ribosome stalling in *TIM50* and other mitoprotein mRNAs, without affecting *TIM50* mRNA levels nor its mitochondrial localization but reducing Tim50 protein levels. (A)** Amino acid sequence alignment of genes encoding Tim50 in *Mus musculus*, *Homo sapiens*, *Schizosaccharomyces pombe*, *Schizosaccharomyces jamonicus*, *Candida lipolytica*, *Candida albicans*, *Saccharomyces cerevisiae*, and *Candida glabrata*. Residues with an asterisk are conserved in all organisms. The region containing the seven consecutive proline residues is highly conserved across yeast species and is marked by a box. **(B)** Wild-type and *tif51A-1* strains containing genomic tagged Tim50-HA were cultured in SGal until post-diauxic phase at 25°C and transferred to 25°C or 37°C for 4 h. Tim50 protein levels were determined by western blotting (left) and quantified (middle). G6pdh levels were used as loading control. A representative image is shown from three independent experiments. *TIM50* mRNA relative levels were determined by RT-qPCR (right). **(C)** Wild-type, *tif51A-1*, and *tif51A-3* strains harboring a FLAG-TIM50-GFP plasmid were cultured in SRaf-URA at 25°C until early exponential phase, transferred to 25°C and 37°C for 2 h, and then transferred to SGal-URA at 25°C and 37°C for three additional hours. Tim50 protein levels were determined by western blotting using a FLAG antibody (left) and quantified (middle). G6pdh levels were used as loading control. A representative image is shown from three independent experiments. *TIM50* mRNA relative levels were determined by RT-qPCR (right). **(D)** Wild-type strain and *tif51A-1* expressing the wild-type Tim50 (left) or Tim50Δ7Pro (right) nLuc constructs were cultured in YPD at 25°C or 37°C for 4 h. One hour after addition of doxycycline to induce nLuc expression, nLuc mRNA relative levels were determined by RT-qPCR. **(E)** Fraction of ribosome reads of various lengths along *YTA12* (left) and *MSS51* (right) transcripts in Schuller et al. (2017) ribosome profiling libraries. **(F)** Wild-type strain and *tif51A-1* were cultured as in B and then subjected to phase contrast and fluorescence microscopy. Mitochondria were visualized by Su9-mCherry and *TIM50* mRNAs were visualized by the single molecule MS2 tag system. A representative image is shown from three independent experiments. Scale bar, 4 µm. **(G)** Wild-type strain and *tif51A-1* expressing Tim50-GFP and Su9-mCherry were cultured in SGal medium at 25°C until reaching post-diauxic phase and subjected to fluorescence microscopy. A representative image is shown from three independent experiments. Scale bar, 4 µm. Arrows indicate *TIM50* mRNA. **(H)** Quantification of Tim50 and Cyc1 aggregates co-localizing with Hsp104 (data from three biological experiments with at least 150 cells quantified). Data obtained from experiments in Fig. 3 I and Fig. 4 J. Data information: In B–D and H, results are presented as mean ± SD from three independent experiments. The statistical significance was measured by using a two-tailed paired Student's *t* test. *P < 0.05, **P < 0.01, ***P < 0.001. The asterisks located above the columns of the graph represent a comparison between different temperatures within the same strain. The asterisks found at the top of the bars additionally indicate comparisons between the indicated strains at the same treatment condition. n.s means no significant differences. Source data are available for this figure: SourceData FS4.

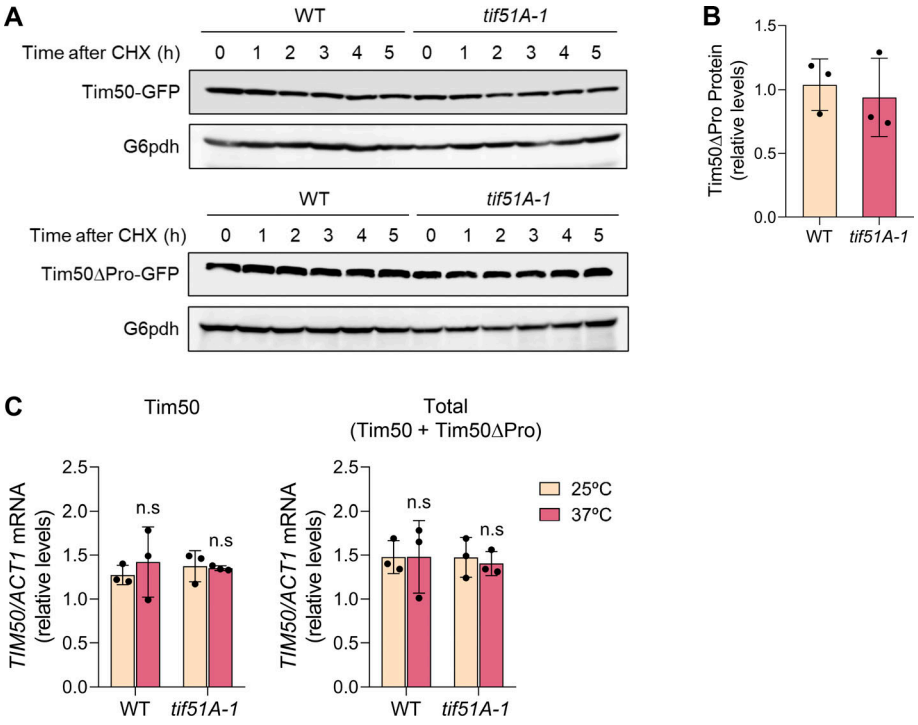

Figure S5. **eIF5A depletion does not affect the half-life of Tim50ΔPro protein nor the expression of the Tim50 and Tim50ΔPro copies. (A)** Wild-type and *tif51A-1* strains harboring Tim50-GFP (up) or Tim50ΔPro-GFP (down) were cultured in SGal medium until reaching post-diauxic phase at 25°C and transferred to 37°C for 4 h. Then cultures were treated with CHX (100 µg/ml) for 5 h and Tim50 protein levels were determined by western blotting using a GFP antibody. G6pdh levels were used as loading control. A representative image is shown from three independent experiments. **(B)** Tim50ΔPro steady-state protein levels were quantified from A. **(C)** Wild-type and *tif51A-1* harboring Tim50ΔPro and an extra copy of wild-type Tim50 were cultured as in A. mRNA relative levels from wild-type *TIM50* (left) and total *TIM50* (wild-type *TIM50* plus *TIM50ΔPro*, right) were determined by RT-qPCR. Data information: In B and C, results are presented as mean ± SD from three independent experiments. The statistical significance was measured by using a two-tailed paired Student's *t* test relative to wild-type strain. n.s means no significant differences. Source data are available for this figure: SourceData FS5.

Provided online are Table S1, Table S2, Table S3, Table S4, Table S5, and Table S6. Table S1 shows mitochondrial proteins detected in the proteomic analysis with a statistically different 41°C/25°C ratio in at least one eIF5A temperature-sensitive mutant with respect to wild-type. Table S2 shows yeast strains used in this study. Table S3 shows the plasmids used in this study. Table S4 shows the oligonucleotides used in this study. Table S5 shows the main characteristics of mRNAs analyzed by polysome profiling. Table S6 shows co-translationally inserted mitoproteins with the largest shift of ribosome distribution upon eIF5A depletion.